ChemComm

FEATURE ARTICLE

View Article Online
View Journal | View Issue

Cite this: *Chem. Commun.*, 2016, **52**, 8935

Bioreductive fluorescent imaging agents: applications to tumour hypoxia

Robert B. P. Elmes

Received 1st February 2016,
Accepted 19th February 2016

DOI: 10.1039/c6cc01037g

www.rsc.org/chemcomm

Large tumours contain regions with very low intracellular O_2 concentrations. Known as hypoxia, this feature of tumours yields a highly reducing environment owing to the presence of numerous oxygen sensitive reductase enzymes. The development of new optical chemosensors for these various reductases presents an ideal approach to visualise areas of hypoxia or highly reducing environments. Critical to the success of such chemosensors is the design of probes containing a bioreductively activated moiety that either ensures the selective retention of fluorescence within a hypoxic tissue or a probe that irreversibly releases a reporter fluorophore. This Feature Article aims to summarise the fluorescent tools that have been developed to image tumour hypoxia and the various reductase enzymes associated with the bioreduction process.

1. Introduction

Hypoxia, a diminished availability of molecular oxygen in bodily tissues, has long been a therapeutic target for cancer research given its major role in tumour development and resistance to therapy.[1,2] The imperfect neovascularisation seen in growing solid tumours results in limited and inefficient blood vessel networks, and leads to the presence of a variable but significant proportion of hypoxic cells.[3] Indeed, since the discovery of Varghese *et al.* in 1976 that 2-nitroimidazoles are capable of forming adducts with cellular nucleophiles in hypoxic cells,[4] hypoxia-activated prodrugs have been the subject of intense investigation culminating with the recent entry of evofosfamide (Fig. 1) into stage 3 clinical trials for pancreatic cancer and soft tissue sarcoma.[5–7]

The proposed activation of 2-nitroimidazoles stems from an initial enzymatic bioreduction resulting in the delivery of an electron to the nitro group yielding a nitro radical. Under aerobic conditions, the nitro radical is back-oxidised to the parent nitro compound by molecular oxygen which is converted to a superoxide anion and subsequently transformed to hydrogen peroxide by superoxide dismutase (SOD).[8] However, in hypoxic regions oxygen pressures can fall to below 2.5 mmHg,[9] inhibiting the back-oxidation of the nitro radical anion and prompting further reduction to nitroso and subsequently hydroxylamine and amine derivatives. This 'unmasking' yields ideal substrates for covalent attachment to intracellular nucleophiles (*i.e.* proteins or DNA) and selective retention in hypoxic cells relative to normoxic cells (Fig. 1a). This reduction process is also exploited by prodrugs such as evofosfamide to trigger release of the active drug molecule (Fig. 1b).

In mammalian cells, a number of different reductase enzymes associated with the cytoplasm, mitochondria, and microsomes have been implicated in the bioreduction of 2-nitroimidazoles. These include one-electron reductases such as NADPH–nitroreductases, NADPH–cytochrome P450 reductase, cytochrome b5 reductase and xanthine oxidase, and two-electron reductases such as DT-diaphorase.[10] Moreover, a host of other functionalities such 4-nitroimidazoles, 4-nitrobenzenes, nitrofurans, azo linkages, tertiary amine *N*-oxides, aromatic di-*N*-oxides and quinones have all been shown to be susceptible to reduction by the various reductase enzymes.[9] In essence, the observed diversity of both enzymes and substrates provides an assortment of tools available not only for the design of hypoxia targeting agents but also to selectively target tissues in which the aforementioned enzymes reside. Indeed, the inextricably linked role of reductase enzymes with hypoxia has boosted research into the development of techniques to accurately detect and profile their function. To date many detection techniques such as ^{19}F NMR, positron emission tomography (PET), single-photon emission computed tomography (SPECT) and immunohistochemistry to name just a few have exploited bioreducible agents.[11]

The bioreduction approach is also particularly amenable to fluorescence detection. Fluorescence signals have been extensively exploited as analytical tools to monitor many biological processes both *in vitro* and *in vivo*.[12,13] Techniques such as confocal microscopy imaging, benefit from high spatial and temporal resolutions where the selective sensing of the desired enzyme enables facile intracellular monitoring and provides valuable information on biological role and functions. Moreover, the potential for

Department of Chemistry, Maynooth University, National University of Ireland, Maynooth, Co. Kildare, Ireland. E-mail: robert.elmes@nuim.ie; Tel: +353 1 7084615

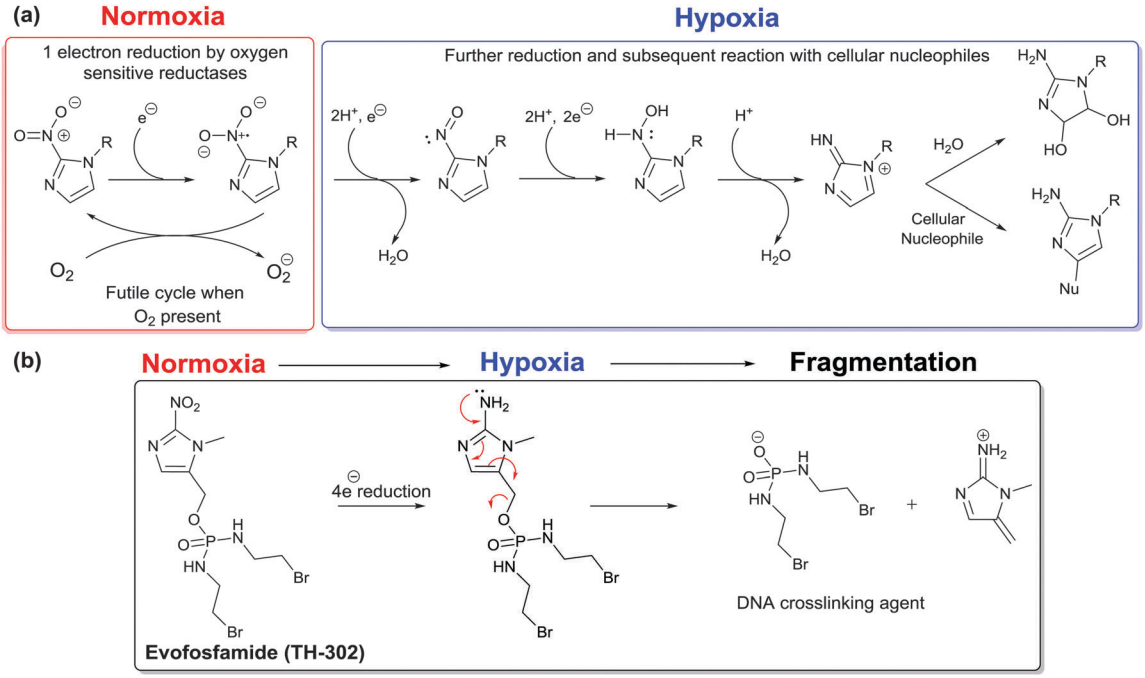

Fig. 1 (a) The proposed oxygen-dependent bioreductive metabolism of 2-Nitroimidazoles and mechanism for selective retention in hypoxic cells. (b) 2-Nitroimidazole containing bioreductive prodrug evofosfamide is activated under hypoxic conditions where reduction leads to fragmentation of the parent drug to release an active DNA crosslinking agent.

'turn on' fluorescent probes brings with it incomparable levels of sensitivity and selectivity and has led to a burgeoning interest in reductively activated fluorescent imaging agents.[14]

This Feature Article aims to be a non-exhaustive summary of the fluorescent tools that have been developed to detect tumour hypoxia and the various reductase enzymes associated with the bioreduction process. It will focus on chemical probes whereby a reduction leads to the release of a fluorescent reporter molecule but also fluorescent probes that are selectively retained in cancerous tissue for imaging applications. The review will not cover oxygen sensing probes or redox active transition metal complexes which have been reviewed elsewhere.[15,16] The bioactivatable probes presented herein exploit various functionalities such as nitroaromatics, azo linkages, quinolones and *N*-oxides among others. It will highlight early attempts to exploit non-fluorogenic nitroaryl substrates up to more recent exploitation of FRET-based azo conjugates. The recent application of similar tools for probing bacterial activity through reductase enzymes will also be described along with some innovative cascade type reactions resulting from bioreduction.

2. Nitroaromatics

The majority of the examples described in this review rely on the reduction of a nitroaromatic moiety present in the structure of a fluorophore. This interest stems from the electron affinity of the nitro functional group and it's ease of reduction by nitroreductase (NTR) enzymes.[17] These flavin-associated oxidoreductase enzymes can be divided into two functional classes. Type I NTRs are oxygen-insensitive, *i.e.* capable of reduction in the presence of molecular oxygen, whereas type II NTRs are oxygen-sensitive and only function under extreme hypoxia.[18] Owing to their role in hypoxia type II NTRs are of particular significance to the design of hypoxia sensitive fluorescent imaging agents.

The early work of Olive and Durand recognised the utility of nitroaromatics for hypoxia imaging where they reported a small family of nitrofurans **1–4** (Fig. 2).[19] They demonstrated that, **1** could be used to estimate the fraction of hypoxic cells in multicellular spheroids where they discovered that the fluorescence intensity of **1** was highly responsive to cellular oxygen concentration. These results presented one of the first studies on the feasibility of nitroheterocycles as hypoxia sensors and several reports followed on the potential applicability of nitrofurans as fluorescent hypoxic cell markers.[20–22]

Further pioneering work was conducted by Hodgkiss, Middleton, Stratford, Wardman and co-workers who published a number of reports on the use of nitroaryl compounds as potential fluorescent probes for hypoxia. After a preliminary screening of a series of compounds with similar structure,[23] their initial investigations focused on the use of nitroakridin 3582,[24] (**5**) and 3-nitronaphthalimide[25,26] (**6**) (Fig. 3) which were shown to be non-fluorescent until reduction of their nitro groups to the corresponding amines resulted in intense fluorescence at 515 nm and 570 nm respectively. They showed, using flow cytometry and HPLC analysis, that both **5** and **6** became highly fluorescent under hypoxic conditions in a number of cell lines but not in the corresponding normoxic cells.[27] However, *in vivo* investigations showed that tumours did not appear to accumulate **5** to any great extent, with levels of <10 μM being

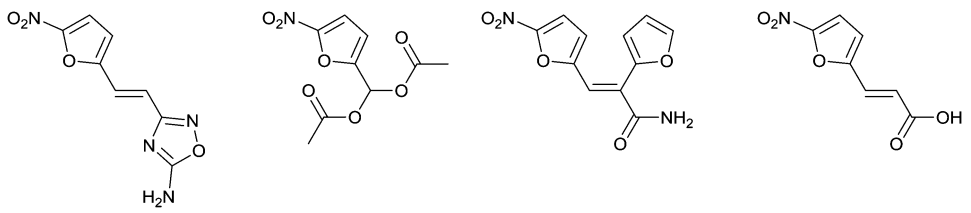

Fig. 2 Nitrofuran derivatives **1–4**.

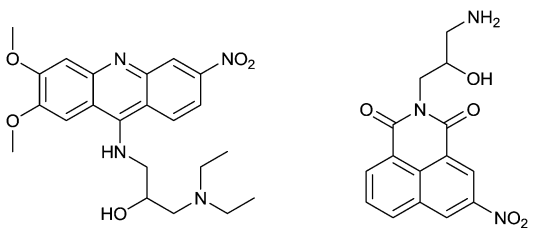

Fig. 3 Nitroaryl compounds **5** and **6**.

observed in the tumours of a male mouse model compared to concentrations of 600 μm being observed in the liver.[26] This large degree of liver accumulation also resulted in significant toxicity where the compound was not tolerated at doses above 0.19 μmol g^{-1}.

A subsequent series of reports focused on compounds having both a 2-nitroimidazole and a fluorescent ring system in their molecular structure (Fig. 4).[28,29] Bioreduction of the nitroimidazole was expected to lead to compounds that would exhibit fluorescence in both normoxic and hypoxic cells but, due to the presence of the reduced nitroimidazole moiety, would be selectively bound in hypoxic cells and thus the fluorescence would be 'fixed' in these cells. The authors prepared a range of compounds based on various fluorophores such as naphthalimide **7**, coumarin **8**, indolizine **9** and bicyclic bimane **10** where **8** and **10** showed more than a 5-fold and 17-fold hypoxic/normoxic fluorescence differential, respectively, when tested in V79 Chinese hamster cells. Hodgkiss later reported an alternative strategy involving biotinylated 2-nitroimidazoles such as **11**.[30] Bioreductively bound adducts of **11** could be clearly detected using either an avidin or streptavidin–FITC conjugate when analysed by flow cytometry and could also be observed in tumour cells of mice which had been exposed to the compound *in vivo*.

Qian and co-workers have explored a number of strategies towards fluorescent markers for hypoxia where their first report focused on 1,8-naphthalimides functionalised with either two 2-nitroimidazole or two 3-nitro-1,2,4-triazole moieties (Fig. 5).[14,31] When evaluated in V79 Chinese hamster, CHO and 95D cells the 2-nitroimidazole compounds **12** and **13** showed a large fluorescence differential between hypoxic and normoxic cells as evidenced by fluorescence microscopy and fluorescence scanning ascent. Indeed, compound **13** showed the largest degree of fluorescence differential with the fluorescence under hypoxic conditions being 20 times as intense as under normoxic conditions.

Derivatives **14** and **15** (Fig. 5) also showed promise as fluorescent markers for hypoxia where both compounds were shown to exhibit increased fluorescence in response to hypoxic conditions in V79 Chinese hamster cells.[32] Similarly to **12** and **13** above, the 2-nitroimidazole compound **15** containing an ether linkage exhibited the largest fluorescence differential where bioreduced **15** exhibited 15 times increased emission compared to it's non reduced nitro analogue.

Qian and co-workers also investigated two series of hypoxia sensors that lacked the 2-nitroimidazole group (Fig. 6).

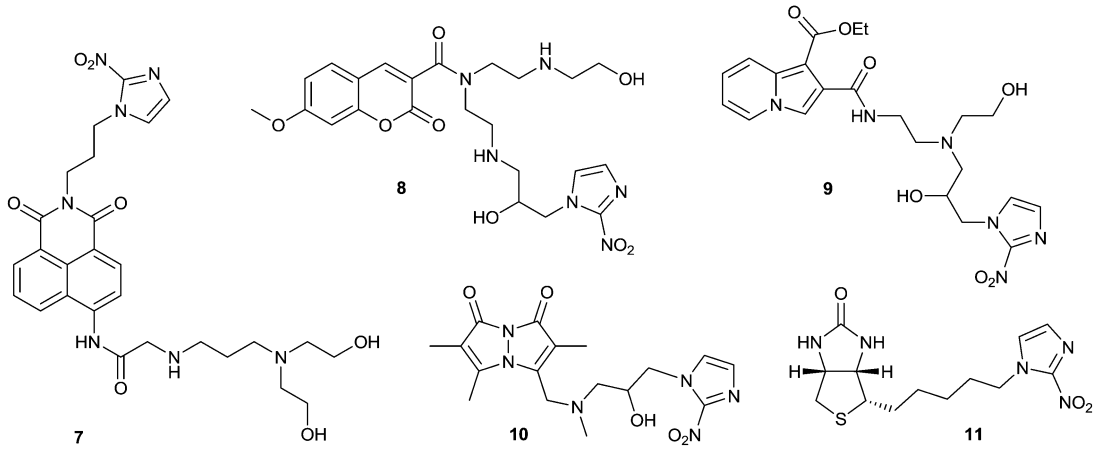

Fig. 4 2-Nitroimidazole conjugates **7–11**.

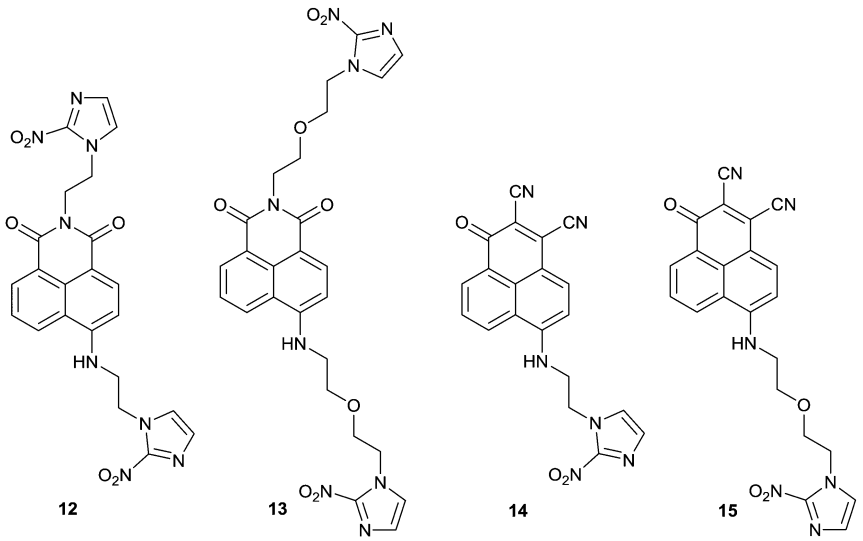

Fig. 5 2-Nitroimidazole–naphthalimide derivatives **12–15**.

This alternative approach was based on either a 7*H*-benzimidazole[2,1-*a*]benz[*de*]isoquinolin-7-one core such as **16** and **17** or on an acenaphtho[1,2-*b*]quinoxaline core such as **18**, **19** and **20**. Compounds **16** and **17** showed particular promise with **16** showing a normoxic/hypoxic fluorescence ratio of 14 when tested in V79 Chinese hamster cells.[33] A similar approach was taken with **18**, **19** and **20**, based on the principle of a quenching nitro-group being reduced under hypoxic conditions. This resulted in hypoxic/normoxic fluorescence differentials of 6, 9, and 11 times with **18**, **19**, and **20** respectively when incubated for 3.5 h in V79 Chinese hamster cells.[34]

The recent development of a ratiometric fluorescent probe for hypoxia saw the synthesis of naphthalimide probe **21**, based on a *p*-nitrobenzyl moiety being conjugated to the naphthalimide fluorophore *via* a carbamate linkage.[35] Using a prodrug approach analogous to that utilised by evofosfamide, this highly selective ratiometric fluorescent sensor was shown to be activated by NTR in the presence of NADH with an obvious blue to green fluorescence shift resulting from release of 4-amino naphthalimide derivative **21a** (Fig. 7). A similar response was observed *in vitro* when the probe was incubated in A549 cells cultured under hypoxic conditions. Moreover, **21** displayed no cytotoxicity thus rendering it a promising candidate as a potential biological imaging agent for hypoxia (Fig. 8).

A similar approach was utilised in the development of **22**, a Nile Blue based long-wavelength fluorescence probe for the detection of NTR which was activated at concentrations as low as 0.1 μM to release the highly fluorescent dye **23**.[36] **22** was found to be both highly sensitive and selective where the detection limit was determined to be 180 ng mL^{-1} of NTR while also being stable towards other biological reductants such as dithiothreitol (DTT), glutathione (GSH), cysteine (Cys) and homocysteine (Hcy) with minimal endogenous interference. Moreover, **22** did not exhibit any cytotoxicity and A549 cells incubated under hypoxic conditions showed a large fluorescence enhancement (Fig. 9).

Nakata, Hori and co-workers designed **24**; a fluorescent pH probe selectively activated under hypoxic conditions.[37] **24** consists of a *p*-nitrobenzyl moiety directly linked to the commercially available xanthene derivative seminaphthorhodafluor (SNARF)

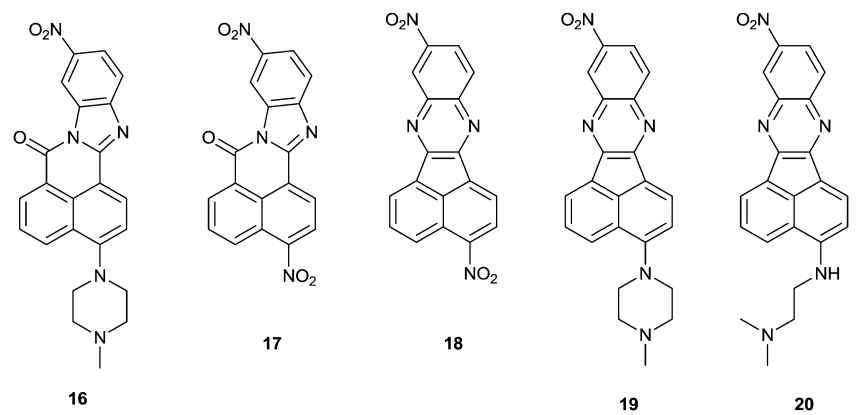

Fig. 6 Nitroaromatic compounds **16–20**.

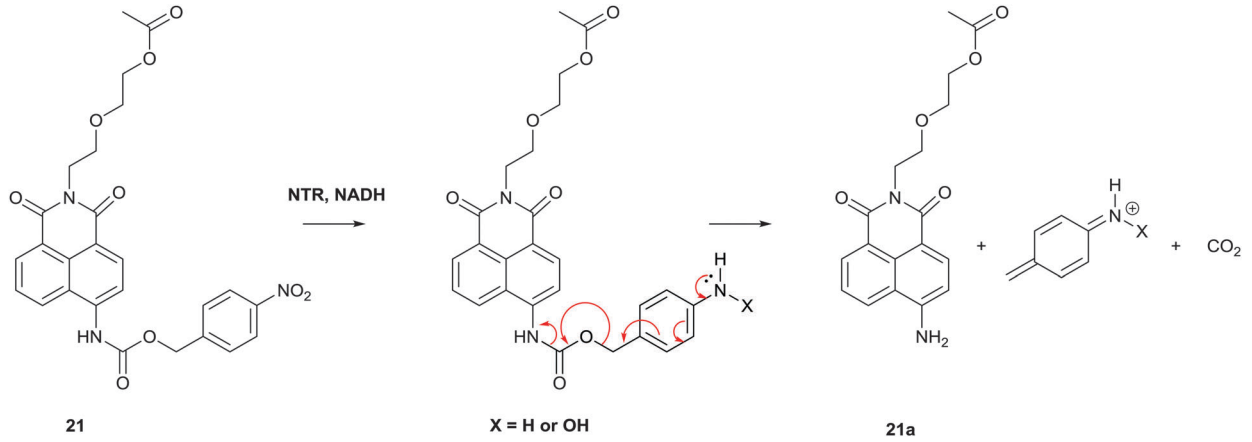

Fig. 7 Conversion of fluorescent sensor **21** to 4-amino-naphthalimide **21a**.

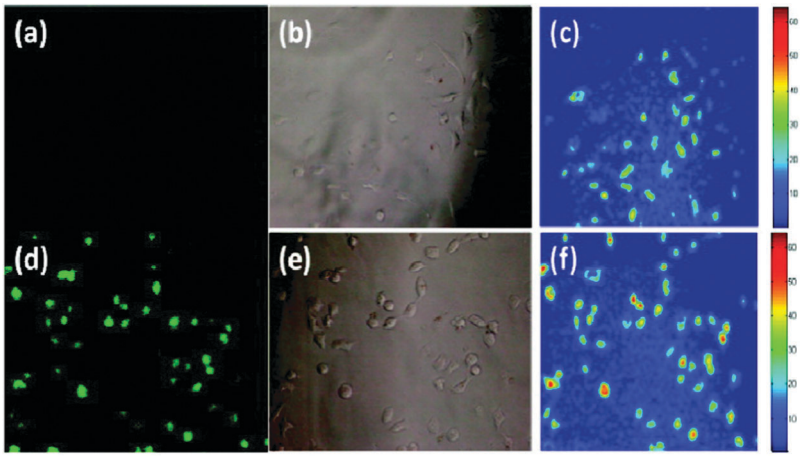

Fig. 8 Fluorescence microphotographs of A549 cells incubated with **21** under normoxic (a–c) and hypoxic (d–f) conditions. (Reproduced with permission from *Org. Lett.*, 2011, **13**, 928–931. © 2011 American Chemical Society).

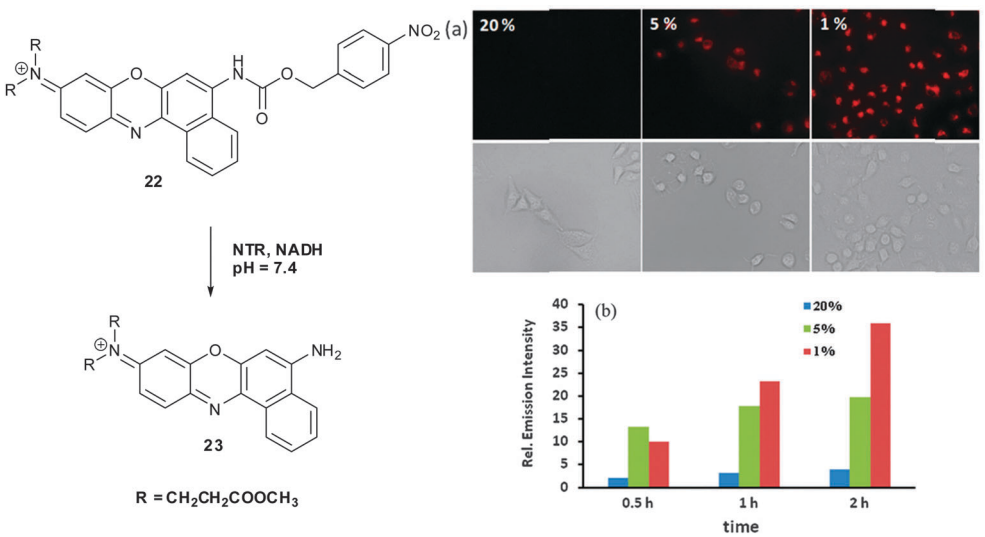

Fig. 9 The conversion of **22** to **23** in the presence of NTR and NADH. (a) Fluorescence microphotographs of A549 cells incubated with **22** under various normoxic and hypoxic conditions. (b) Mean fluorescence intensity change of A549 cells incubated with **22** under various normoxic and hypoxic conditions. (Reproduced from *Chem. Commun.*, 2013, **49**, 10820–10822. © 2013 Royal Society of Chemistry).

through an ether linkage. Reduction of the *p*-nitrobenzyl moiety by either NTR or chicken embryo liver microsomes under hypoxic conditions led to the release of SNARF which was capable of acting as a fluorescent pH indicator (Fig. 10). Moreover, fluorescent imaging of V79 Chinese hamster cells revealed that **24** was strongly fluorescent in the cytosol of cells incubated under hypoxic conditions while negligible fluorescence was observed in the cells treated under aerobic conditions.

Jayagopal and co-workers developed two hypoxia-sensitive imaging agents, **25** and **26**, based on 2-nitroimidazole fluorescein isothiocyanate (FITC) conjugates (Fig. 11).[38] **26** in particular was shown to be effective in human Müller cells at low concentration (10 μM) where a 32-fold greater fluorescence intensity was measured in hypoxic cells when compared against normoxic cells; a demonstration of its ability to be selectively retained in hypoxic retinal cells. Furthermore, intraocular administration

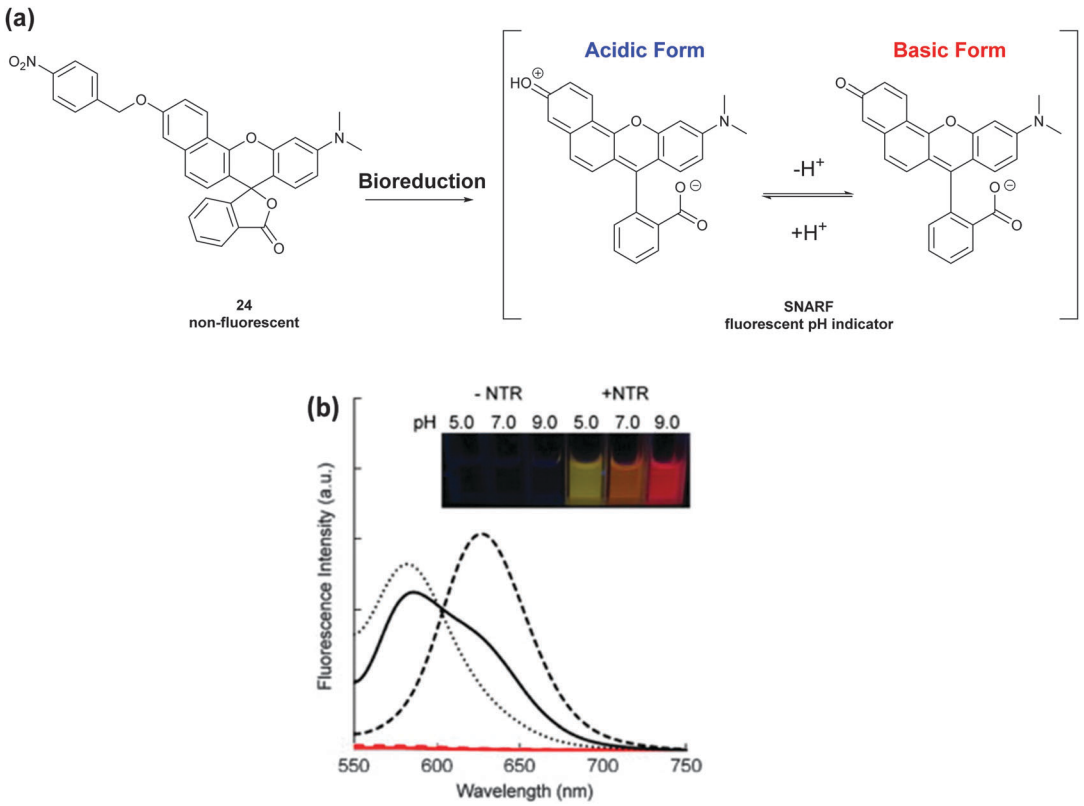

Fig. 10 (a) Bioreduction of **24** to releases the pH responsive fluorophore SNARF. (b) The fluorescence spectra of **24** in the presence (black) or absence (red) of NTR at pH 5.0 (dot line), pH 7.0 (solid line) and pH 9.0 (dashed line). Inset: Photograph of the ratiometric fluorescent response to different pH conditions with or without NTR. (Reproduced with permission from *Bioorg. Med. Chem.*, 2009, **17**, 6952–6958. © 2009 Elsevier).

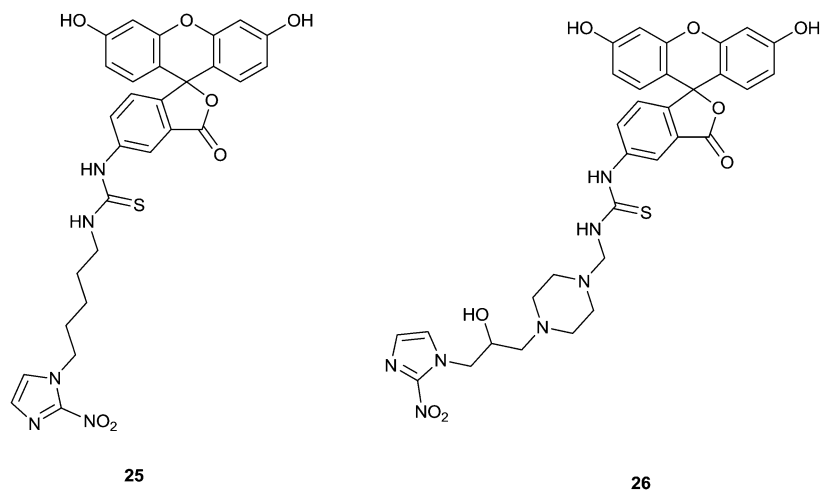

Fig. 11 2-Nitroimidazole fluorescein isothiocyanate conjugates **25** and **26**.

of **25** and **26** in mouse models of retinal hypoxia enabled *ex vivo* imaging of dissected retinae where accumulation of intravitreally injected **25** and **26** in hypoxic areas were clearly observed. These results demonstrated the clear utility of these probes for studying the role of hypoxia in retinal diseases in addition to other tissues featuring hypoxic regions.

Paulmurugan and co-workers demonstrated the utility of CytoCy5S©**27** to track NTR-mediated gene expression both *in vitro* and *in vivo* (Fig. 12).[39] **27** is a quenched substrate of NTR owing to the presence of two nitro substituents, however, upon reduction by cellular NTR **27** became intensely fluorescent at 638 nm. The authors demonstrated the utility of such an approach where they successfully monitored NTR gene expression in NTR transfected cells and also in NTR positive tumour xenografts in live nude mice using fluorescence imaging. Gjertsen and co-workers developed a squaraine analogue **28** for similar applications where their methodology allowed evaluation of NTR gene directed enzyme prodrug therapy (GDEPT) with a well-known antibiotic metronidazole without interference of the therapeutic potential (Fig. 12).[40] This approach perfectly exemplified the broad potential clinical applications for this approach in terms of both imaging and gene therapy.

Nagasawa and co-workers developed two 2-nitroimidazole-tricarbocyanine conjugates **29** and **30** (Fig. 13).[41,42] Unlike previous examples that displayed a fluorescence 'switching on' effect, both **29** and **30** displayed fluorescence quantum yields of 0.18 and 0.05 respectively in their quiescent state. However, upon bioreductive activation of the 2-nitroimidazole moiety, selective binding and accumulation of both dyes occurred preferentially in hypoxic cells over normoxic cells as evidenced by fluorescence microscopy. *In vivo* fluorescence imaging also specifically detected **29** and **30** in subcutaneous tumours of nude mice inoculated with SUIT-2/HRE-Luc cells. Interestingly, *ex vivo* immunohistochemical analysis of the excised tumours also revealed a strong correlation between **29** and areas expressing the well-known hypoxia marker hypoxia inducible factor 1α (HIF 1α) suggesting the potential application of **29** as an *in vivo* optical imaging probe.

Smith, Zhu and co-workers have pursued an analogous approach to hypoxia imaging with a number of reports detailing their efforts towards imidazole–indocyanine green conjugates **31–35** (Fig. 14). Their first generation fluorophore **31** was shown to display a large contrast in fluorescence intensity (2.5 fold)

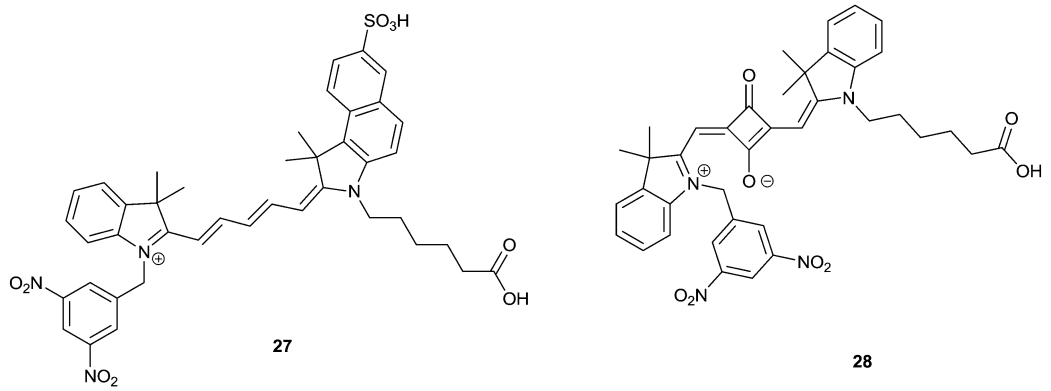

Fig. 12 Cyanine and squaraine based fluorescent sensors **27** and **28**.

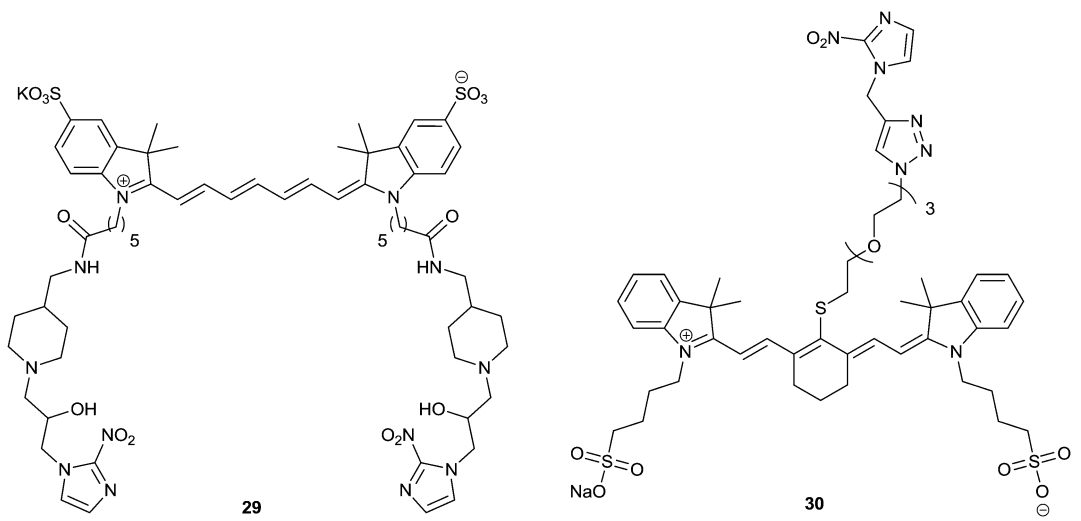

Fig. 13 2-Nitroimidazole–cyanine conjugates **29** and **30**.

between 4T1 breast cancer cells treated under hypoxic and normoxic conditions.[43] Moreover, when measured in an *in vivo* tumour model, **31** was also shown to exhibit two-fold higher fluorescence at the tumour site when compared against the untargeted dye **32**.[44] A subsequent report detailed the synthesis and evaluation of the more metabolically stable fluorophore **33** where the labile ester linkage was replaced by a more robust piperazine moiety.[45] Fluorescence tomography analysis of mouse tumours revealed that **33** showed 2-fold higher fluorescence in hypoxic tumours relative to **31**, within three hours post-injection while it was measured as 1.6–1.7 times higher beyond 3 hours. A more recent article reported the synthesis and evaluation of a third generation dye **34** where the polyene linker had been reduced in length by two carbon atoms.[46] With a more planar and rigid structure, **34** displayed markedly different photophysical characteristics showing absorption and emission maxima of 657 nm and 670 nm respectively; shifted ~100 nm from the maxima of **33** (755 nm and 780 nm respectively). **34** also displayed a fluorescence quantum yield of 0.467 (5 times higher than that of **33**) which resulted in more than two times the average *in vivo* fluorescence intensity being measured for **34** when compared to **33** in a mouse tumour even though **33** was retained in the tumour to a greater extent. Utilising the considerably more cost effective 4-nitroimidazole moiety Smith, Zhu and co-workers also recently reported the preparation of the 4-nitroimidazole–piperazine–indocyanine derivative **35**.[47] The introduction of a 4-nitroimidazole moiety was shown to not significantly affect the retention of the dye in tumours where, in fact, **35** showed a 1.5-fold higher fluorescent intensity after 15 min post-injection compared to **33** when measured in BALB/c tumour-bearing female mice. However, there are some concerns around the toxicity of 4-nitroimidazole containing compounds[48] thus further research is on-going to determine any toxic effects associated with **35**.

Tang and co-workers developed the 2-nitroimidazole tricarbocyanine conjugate **36** as a probe for intracellular hypoxia (Fig. 15).[49] Treatment of **36** with rat liver microsomes known to contain several reductase enzymes produced a strong absorption peak at 695 nm and concomitant fluorescence emission at 750 nm. Moreover, **36** was found to be highly selective for NTR, non-toxic and displayed a detection limit of 77 ng mL^{-1}. Using **36** as a marker for hypoxia, the authors revealed that under hypoxia HepG2 cells exhibit down-regulation of E-cadherin expression with concomitant up-regulation of α smooth muscle actin (α-SMA) expression; two known markers of the epithelial–mesenchymal transitions (EMTs) in tumour migration.

Shi *et al.* used a similar approach where they reported the synthesis of the *p*-nitrobenzyl–cyanine derivative **37** (Fig. 15).[50] NTR was found to reduce the aromatic nitro group causing self-immolative fragmentation and resulting in restoration of π-electron conjugation yielding a ~50-fold fluorescence emission enhancement at 708 nm (Fig. 16). Like **36**, **37** was shown to be highly selective for NTR where other biological reductants such glutathione, cysteine, homocysteine and dithiothreitol did not cause any noticeable changes in emission.

Feng, Li and co-workers recently reported an ultrasensitive method for *in vivo* NTR imaging based on nitroaryl–cyanine conjugates **38–42** (Fig. 17).[51] Of the compounds synthesised, only **38** showed appreciable sensitivity to NTR thought to be a result of enzyme substrate specificity where **39–42** could not approach the active site of NTR in a favoured spatial arrangement.

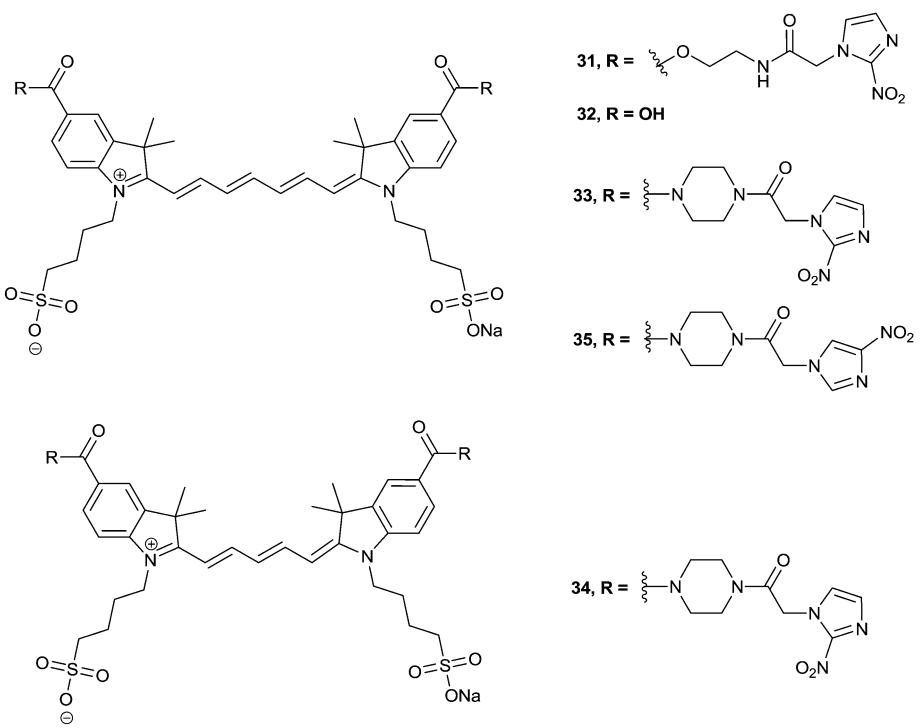

Fig. 14 Nitroimidazole–indocyanine green conjugates **31–35**.

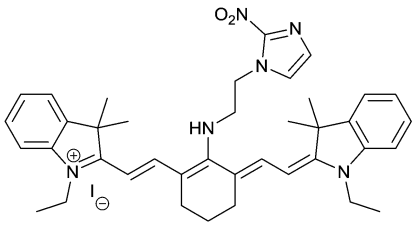

36

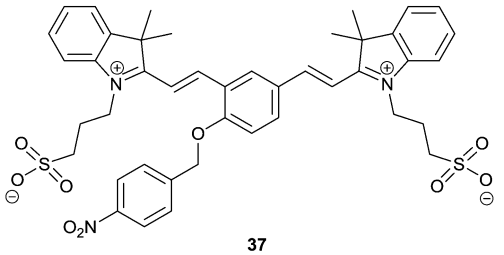

37

Fig. 15 Cyanine derivatives **36** and **37**.

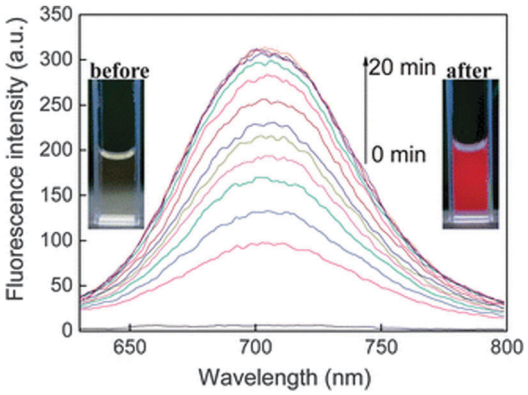

Fig. 16 The fluorescence response of **37** to NTR in the presence of NADH. The insets depict the fluorescence change to the naked eye under UV irradiation. (Reproduced from *Analyst*, 2013, **138**, 1952–1955. © 2013 Royal Society of Chemistry).

In contrast, **38** showed a fluorescence quantum yield of $<0.1\%$ before bioreduction but in the presence of NTR and NADH gave rise to a 110-fold fluorescence emission enhancement in the NIR region (λ_{max} = 782 nm) and a detection limit of 1.14 ng mL^{-1}. *In vitro* imaging of hypoxic A549 cells at various oxygen concentrations (20%, 10%, 5%, 3% and 1%) demonstrated the ability of **38** to act as an *in cellulo* imaging agent for hypoxia. Furthermore, time course *in vivo* fluorescence imaging of an A549 mouse tumour model revealed NIR fluorescence within 2 seconds of injecting **38** with an 8-fold higher intensity measured inside the tumour within 3 minutes (Fig. 18).

Sha, Zhang and co-workers recently reported the synthesis of **43** (Fig. 19), an analogous cyanine based 'turn on' fluorescent probe for NTR.[52] Taking advantage of a nitrobenzyl trigger, **43** demonstrated a highly sensitive and selective response to NTR *in vitro* culminating in an 80-fold fluorescence increase at 720 nm upon exposure to NTR and NADH. Similarly, **43** was also capable of imaging HeLa cells under hypoxic conditions (1% O_2) while under normoxic conditions (20% O_2) no fluorescence was detected.

Jiang and co-workers described the cyanine derived ratiometric probe **44** (Fig. 20).[53] **44** displayed characteristic fluorescence emission at 805 nm, however, upon bioreduction in the presence of NTR and NADH a decrease in fluorescence intensity at 805 nm was observed with the concomitant appearance of a blue-shifted emission band at 747 nm. HRMS-ESI analysis revealed that such changes were a result of bioreduction of the *p*-nitrobenzyl moiety followed by a 1,6-elimination/decarboxylation mechanism releasing dye **45**. Moreover, **44** was found to be highly selective and sensitive exhibiting a calculated detection limit of 0.0058 ng mL^{-1}; the lowest detection limit for NTR reported to date. Cell imaging studies revealed that **44** was also capable of distinguishing between hypoxic and normoxic cells by dual-emission ratiometry.

A semi-cyanine fluorophore **46** has also been utilised by Qian and co-workers for the detection of NTR and hypoxia (Fig. 21).[54] This selective turn-on fluorescent probe is activated by NTR where reduction of a *p*-nitrophenyl to a *p*-aminophenyl group leads to restoration of the pull–push electronic system of the semi-cyanine. Such reduction resulted in an 85 fold fluorescence emission enhancement at 556 nm with a detection limit of 40 ng mL^{-1} within 30 minutes. The probe, while exhibiting little cytotoxicity to A549 cells, was also capable of *in vitro* imaging of these cells under hypoxia. A549 cells treated with **46** under normoxic conditions showed no appreciable fluorescence, however, at 1% oxygen an increase in red fluorescence was clearly observed.

Ma and co-workers synthesised a resorufin based fluorophore **47** utilising 5-nitrofuran as a hypoxia sensitive trigger (Fig. 22).[55] **47** detected NTR through bioreduction resulting in a 1,6-rearrangement-elimination mechanism that released resorufin giving rise to both colourimetric (colourless to pink) and fluorescence (non-fluorescent to intense red fluorescence) modulations. Again, **47** was shown to be both highly selective and sensitive for NTR (detection limit = 27 ng mL^{-1}) and displayed a non-toxic biological profile. Through it's sensitivity for NTR, **47** was used to image A549 and HeLa cells under different extents of hypoxia using confocal microscopy. No considerable fluorescence was observed from cells under normoxia (20% O_2) while fluorescence intensity at 585 nm increased in response to decreasing levels of O_2 from 20% to 1%. An analogous approach was used by the same group where the related 5-nitrothiophene derivative **48** was also shown to act as an 'off–on' fluorescence probe for NTR (Fig. 22).[56] **48** showed similar selectivity towards NTR but with higher sensitivity (detection limit = 0.2 ng mL^{-1}) and, interestingly, was capable of quantitatively determining the concentration of NTR produced by *Escherichia coli* in culture; the first such example with potential for real-time and quantitative determination of NTR in biological organisms.

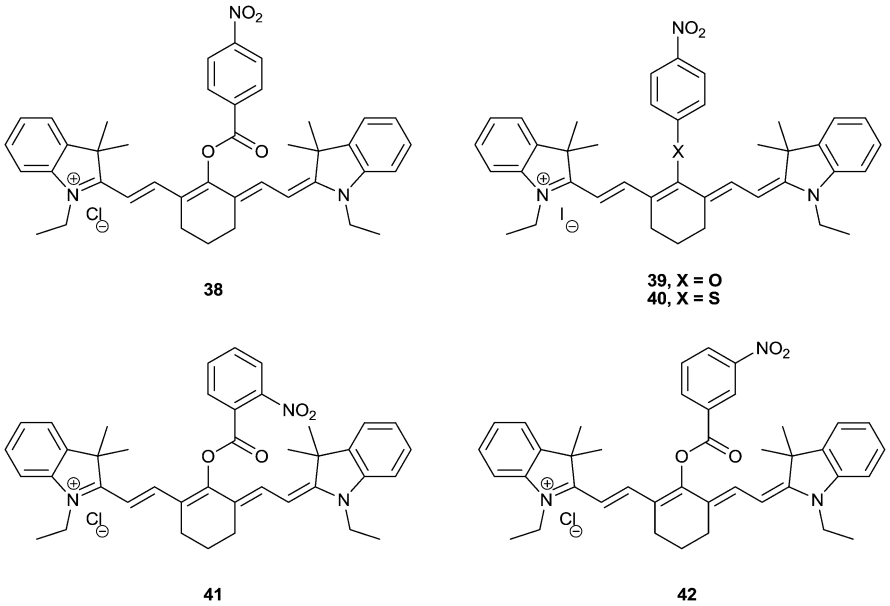

Fig. 17 Nitroaryl–cyanine conjugates **38–42**.

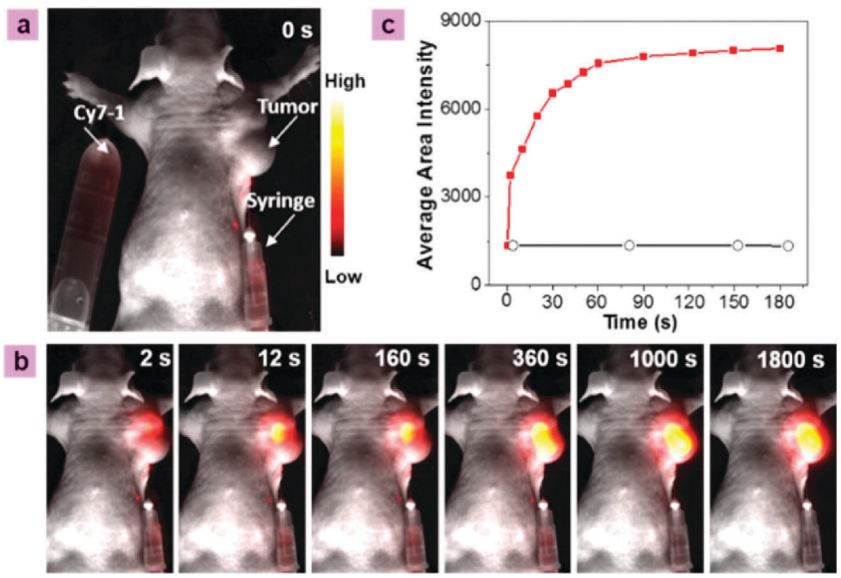

Fig. 18 *In vivo* fluorescence imaging of an A549 tumour model (a) before and (b) after injecting **38**. (c) The fluorescence time-course experiment of **38** in solution (black) and upon exposure to the tumour region (red) from 0 to 180 seconds after injection. (Reproduced with permission from *J. Am. Chem. Soc.*, 2015, **137**, 6407–6416. © 2015 American Chemical Society).

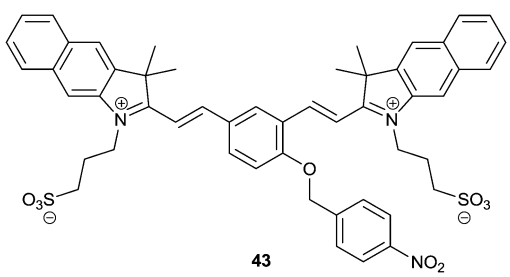

Fig. 19 Nitrobenzyl–cyanine conjugate **43**.

Ma and co-workers pursued an alternative fluorophore in their subsequent report which took advantage of a cresyl violet based probe **49** for the detection of NTR in both MCF-7 cells and zebrafish (Fig. 23).[57] As in previous reports NTR was shown to catalyse the reduction of a nitroaromatic moiety within the probe structure resulting in a large fluorescence enhancement at 625 nm. **49** detected NTR in aqueous solution with high selectivity and sensitivity (detection limit = 1 ng mL^{-1}) and also displayed intense fluorescence within hypoxic MCF7 cells. Moreover, cells cultured in 5% and 1% O_2 were shown to display

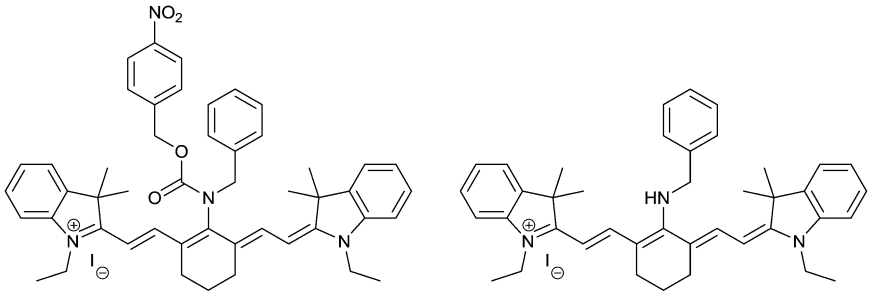

44 45

Fig. 20 Cyanine derived probe **44** and reduction product **45**.

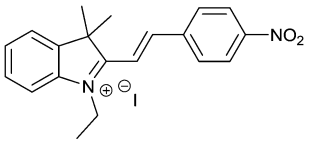

46

Fig. 21 Semi-cyanine fluorophore **46**.

1.6 and 3 times stronger fluorescence respectively when compared against normoxic cells; indicating that endogenous NTR levels increase in response to a decrease in O_2 concentration. Exploratory experiments using **49** also indicated the presence of endogenous NTR in zebrafish embryos where, interestingly, fluorescence microscopy suggested a non-uniform distribution of NTR in this organism. A subsequent report aimed to clarify this effect with the design and synthesis of **50** (Fig. 23), a new fluorescent probe with 'off–on' properties displaying maximum fluorescence at 670 nm.[58] Similar to Ma's previous examples **50** displayed exquisite selectivity over other biological interferents, good sensitivity towards NTR (detection limit = 14 ng mL^{-1}) and good biocompatibility when measured in HeLa cells. Fluorescence imaging of zebrafish embryos treated with **50** displayed intense and non-uniform fluorescence implying that **50** localises to specific tissues within the zebrafish but also confirming the findings of their previous report that suggested the presence of endogenous NTR. Confirmation of this was attained by treating the same zebrafish with the known NTR inhibitor dicoumarol which resulted in a significantly weaker fluorescence signal than that from the untreated animal; an indication that dicoumarol was effectively inhibiting the activity of endogenous NTR (Fig. 24).

BODIPY based probe **51**, a quaternarised 4-pyridinyl-substituted fluorophore conjugated to 5-nitrofuran was developed by Shao, Li and co-workers (Fig. 25).[59] Bioreduction of the nitrofuran moiety by NTR in the presence of NADH was found to release the 4-pyridinyl BODIPY dye **52** resulting in a concomitant 20-fold increase in fluorescence intensity at 520 nm. Furthermore, **51** was found to be a selective and sensitive probe being stable to a number of interferants (NaCl, KCl, $CaCl_2$, $MgCl_2$, cysteine, glutathione, dithiothreitol, glutamic acid, arginine, vitamin C, vitamin B6, H_2O_2, HClO, glucose and human serum albumin) while also displaying a detection limit of 9.6 ng mL^{-1}. Being highly sensitive to NTR **51** was also shown to be amenable to biological application where it was used to track the quantities of NTR produced by *E. coli* in culture and also to act as a

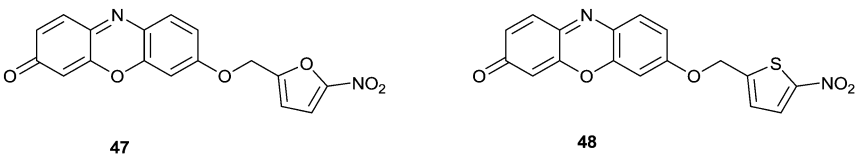

47 48

Fig. 22 Resorufin based fluorophores **47** and **48**.

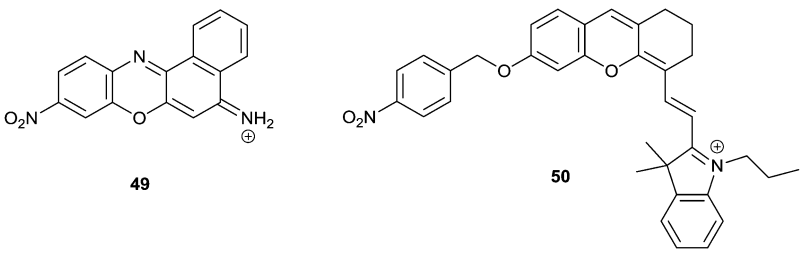

49 50

Fig. 23 Cresyl violet and semi-cyanine based probes **49** and **50**.

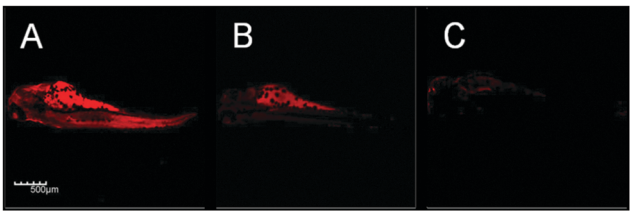

Fig. 24 Fluorescence images of NTR in living 3-day-old zebrafish. (A) Zebrafish treated with bioreduced **50**, (B) zebrafish treated with **50** (C) zebrafish pre-incubated with dicoumarol inhibitor and subsequently treated with **50**. Scale bar, 500 μm. (Reproduced with permission from *Biosens. Bioelectron.*, 2015, **63**, 112–116. © 2015 Elsevier).

sensitive fluorescent imaging agent for hypoxic A549 cells human epithelial lung carcinoma cells. More recently, another BODIPY based probe **53** has been reported as a 'turn-on' fluorescent probe for hypoxic cell imaging (Fig. 25).[60] Using time-dependent density functional theory (TD-DFT) calculations, the authors discovered that the presence of a nitrohydroxy-phenyl ring resulted in a nonradiative decay of the S_1 excited state of **53** with subsequent reduction of the nitro group leading to a recovery of fluorescence. This finding was confirmed in a biological context where HeLa cells treated with **53** under normoxic conditions showed negligible intracellular fluorescence while cells incubated with under hypoxic conditions produced significant intracellular between 550 and 650 nm (Fig. 26).

Recently Debieu and Romieu reported innovative dual enzyme-responsive sensors **54–56** based on the *in situ* formation of 7-hydroxy-2-iminocoumarins (Fig. 27).[61] The "AND" fluorogenic molecular logic gate design concept employed allowed simultaneous fluorogenic detection of hydrolase and reductase enzymes. Double activation through both hydrolysis of an amide (or ester) bond and nitro-reduction, followed by a 1,6-elimination/cyclisation gave fluorescence at 489 nm caused by release of 7-hydroxy-(2-imino)-coumarin species. The coumarin fluorophore was also exploited by Mishra and co-workers who reported the synthesis of two coumarin–nitroimidazole conjugates **57** and **58** (Fig. 27).[62] **57** in particular was shown to be selectively retained in hypoxic cells exhibiting a 10 fold fluorescence increase in flow cytometry experiments with a negligible signal being observed in normoxic cells.

Jiang, Tan and co-workers reported the nitro-substituted benzothiadiazole probe **59** capable of labelling hypoxic cells with

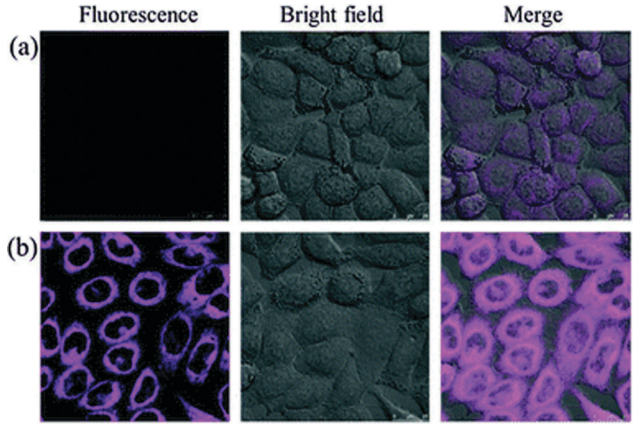

Fig. 26 Confocal fluorescence microscopy images of HeLa cells treated with **53** (a) HeLa cells under normoxic conditions and (b) HeLa cells under hypoxic conditions. (Reproduced from *Chem. Commun.*, 2015, **51**, 13389–13392. © 2015 Royal Society of Chemistry).

'switched on' fluorescence at 600 nm in response to bioreduction (Fig. 28).[63] **59** showed no cytotoxicity to human osteosarcoma MG63 cells and effectively labelled 65% of cells grown under hypoxic conditions in comparison to only 2.4% under normoxic conditions as evidenced by flow cytometry analysis.

In an unexpected revelation Gates and co-workers reported the hypoxia selective enzymatic conversion of 6-nitroquinoline **60** into the fluorescent helicene **61** (Fig. 29).[64] Although expecting the simple bioreduction of **60** to yield 6-aminoquinoline, fluorescence and LC-MS analysis revealed that one-electron reduction by cytochrome P450 reductase in the presence of NADPH under hypoxia actually resulted in the formation of azoxy-helicene product **61** giving rise to a 63-fold increase in fluorescence at 445 nm.

A subsequent report from the same group did report the enzymatic conversion of **60** to **62** under hypoxic conditions (Fig. 29); this time using the xanthine/xanthine oxidase enzymatic reducing system under hypoxic conditions.[65] Wilson and co-workers investigated a series of quinolone compounds and reported that 6-nitroquinolone ester **63** (Fig. 29) had a high anoxic/oxic fluorescence differential (~400–500-fold) and behaved as a fluorescent probe for cytochrome P450 oxidoreductase and other NADH dependant reductases under hypoxic conditions.

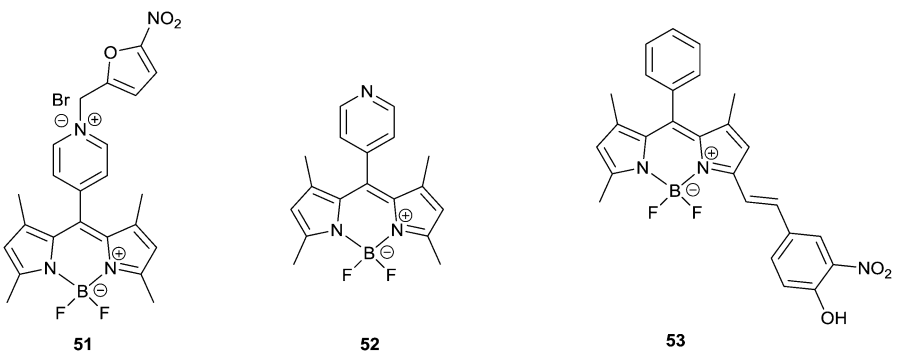

Fig. 25 BODIPY based probes **51–53**.

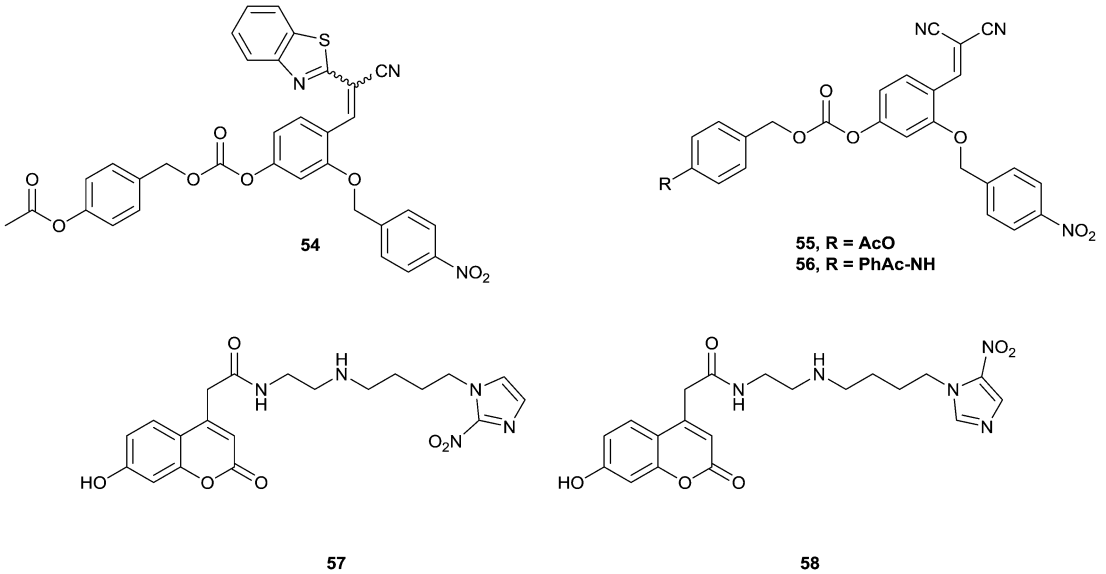

Fig. 27 Dual enzyme-responsive sensors **54–56** and coumarin–nitroimidazole conjugates **57** and **58**.

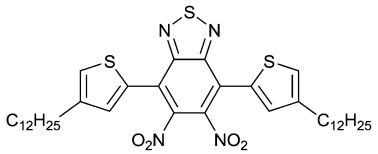

Fig. 28 Nitro-substituted benzothiadiazole probe **59**.

Moreover, the *in vitro* metabolism of **63** showed significant correlation with that of PR-104A,[66] the known dinitrobenzamide prodrug, where both were similarly activated in 22 different human tumour cell lines as evidenced using fluorescence microscopy and flow cytometry.[67]

The nitroimidazole–ruthenium conjugate **64** (Fig. 30), one of the few metal based examples in this review, was reported by Suzenet, Brindell and co-workers and was found to be selectively retained in hypoxic over normoxic A549 cells.[68] The luminescence properties of **64** were highly sensitive to the environment where binding to human serum albumin (HSA) resulted in an emission increase and a lengthening of the luminescence lifetime (490 ns to 809 ns and 895 ns) while binding to calf thymus DNA resulted in an emission decrease of 65% and a shortening of the luminescence lifetime (660 ± 10 ns to 540 ± 10 ns). Complex **64** was also found to be highly cytotoxic to cells and thus not applicable as an imaging agent. A subsequent study by the same authors examined the biological properties of **64** in detail where the complex was found to possess higher potency than cisplatin *in vitro*.[69]

Recently, Liang, Zhang and co-workers reported **65** (Fig. 30), a high sensitivity probe for monitoring NTR activity, utilising both one-photon and two-photon fluorescence.[70] **65** exhibited a NTR-induced fluorescence enhancement of *ca.* 70-fold and a detection limit of 20 ng mL^{-1}. Moreover, **65** was capable of imaging hypoxic cells with little observed cytotoxicity and high differentiation between hypoxic and normoxic cells. Imaging of rat liver tissue slices also exhibited the applicability of **65** to tissue hypoxia monitoring where it was employed to successfully image tissue at imaging depths of 70–160 μm.

Bacterial imaging has also emerged as a potential application for bioreductively responsive probes due to the inherent production of NTR, both type I and type II, by many species of bacteria.[71] Tangney and co-workers at University College Cork sought to take advantage of NTR enzymes as a non-invasive reporting strategy for bacterial infection.[72] Initial proof of concept studies utilised the previously described CytoCy5S©**27** in a mouse model where infected mice showed localised fluorescence only in organs infected with bacteria. Moreover, mice

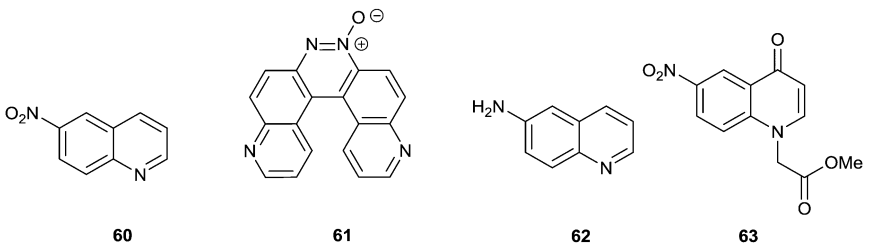

Fig. 29 6-Nitroquinoline derivatives **60–63**.

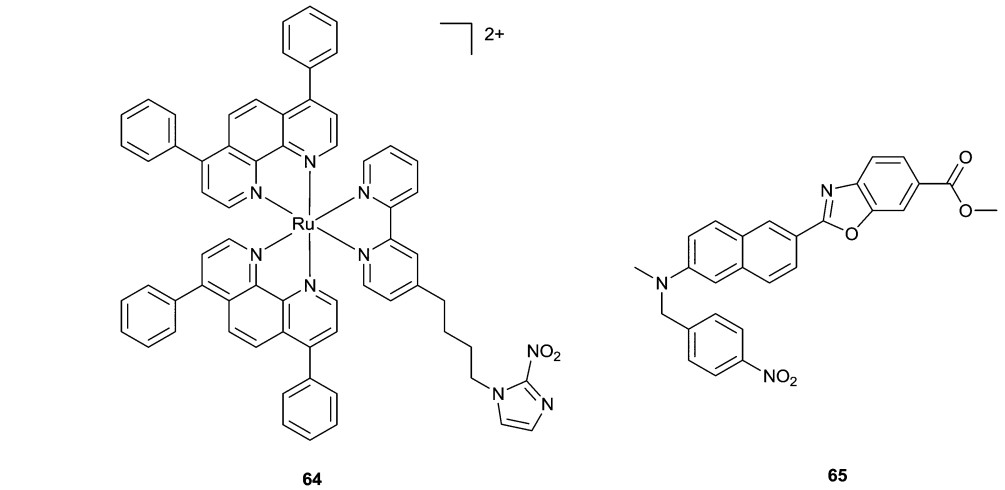

Fig. 30 Nitroimidazole–ruthenium conjugate **64** and nitrobenzyl conjugate **65**.

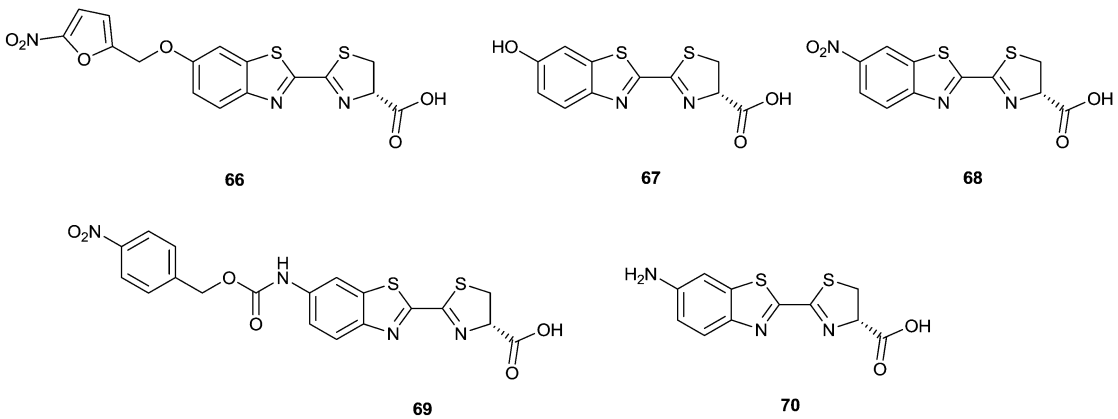

Fig. 31 NTR responsive bioluminescent probes **66–70**.

bearing subcutaneous tumours that had been colonised with *E. coli* also showed selective fluorescence localised within the tumour while those that were not infected showed a negligible fluorescence signal. A subsequent report from Tangney, Dubikovskaya and co-workers described a new NTR responsive bioluminescent probe **66** that was selectively 'switched on' by releasing luciferin **67** in the presence of numerous NTR expressing *E. coli* strains (Fig. 31).[73] **66** also successfully demonstrated high efficiency release of luciferin in an *in vivo* subcutaneous xenograft model where a tumour induced by NTR and luciferase expressing MDA-MB-231 human breast adenocarcinoma cells exhibited intense bioluminescence when treated with the dye.

Luciferin was also exploited in a recent communication from Prescher and co-workers where **68** was employed as a 'caged' luminophore utilising NTR activity to visualise cell–cell contacts (Fig. 31).[74] The nitroaryl group of **68** prevented luminescence through electron-withdrawing effects however upon bioreduction in the presence of NTR, the resulting hydroxylamine was sufficiently electron rich to give a luciferin analogue that could be oxidised by luciferase to yield bioluminescence. Moreover, the authors were able to directly image cell–cell contacts where cells expressing NTR (activator cells) in direct contact with cells expressing luciferase (reporter cells) were easily imaged upon treatment with **68** while those separated by just 1 mm produced negligible luminescence.

The bioluminescent approach was also recently taken by Au-Yeung and co-workers where they reported the synthesis of luciferin derivative **69** (Fig. 31).[75] The approach relied on an aminoluciferin conjugated to a 4-nitrobenzyl carbamate group which, upon bioreduction in the presence of NTR, yielded aminoluciferin **70**. When treated with NTR in the presence of NADH and luciferase **69** gave rise to a 100-fold luminescence enhancement in just 5 minutes. This effect was also applied in the detection of microbial NTR activity across a range of both gram positive and gram negative bacteria demonstrating the potential of **69** as a sensitive, real time probe for the detection of microbial growth.

Stanforth and co-workers have reported several classes of nitroaryl–benzothiazole, benzimidazole and benzoxazole derivatives as fluorescent probes to detect NTR activity in clinically important bacteria (Fig. 32).[76,77] Derivatives such as **71** and **72** were shown to function as indicators of NTR activity across a

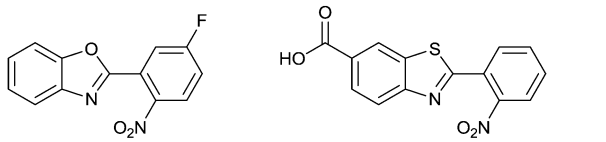

71 72

Fig. 32 Nitroaryl–benzoxazole and benzothiazole derivatives **71** and **72**.

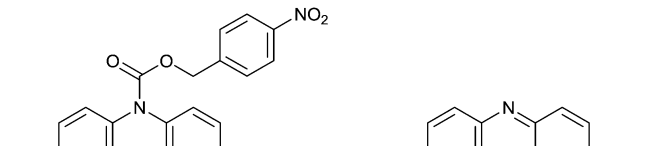

73 74

Fig. 33 Methylene blue based fluorescent probe **73** and the reduction product **74**.

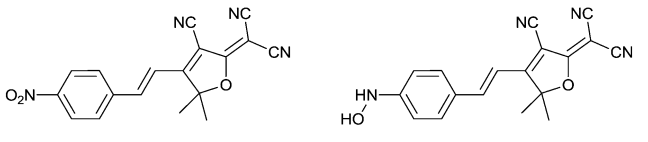

75 76

Fig. 34 Dicyanomethylenedihydrofuran based fluorophores **75** and **76**.

range of both gram negative and gram positive bacteria where strong blue fluorescence was observed upon incubation with bacteria in culture.

A methylene blue based fluorescent probe **73** has recently been reported for NTR detection by Jo and co-workers (Fig. 33).[78] Through a NTR catalysed 1,6-elimination to yield methylene blue **74**, **73** was demonstrated as a sensitive and selective probe for NTR giving rise to 'turn on' fluorescence with λ_{max} = 680 nm. **73** was also investigated as an imaging probe for bacteria where it was demonstrated to undergo a concentration dependent increase in fluorescence intensity in response to *E. coli* growth. Moreover, singlet oxygen production of **73** was also found to be 'switched' in the presence of NTR demonstrating that **73** may also find application as an enzyme triggered photodynamic therapy (PDT) agent.

Moerner and co-workers reported the dicyanomethylenedihydrofuran (DCDHF) based fluorophore **75** (Fig. 34) in the development of enzymatic turnover-activated localisation microscopy (ETALM); a super-resolution imaging technique based on single-molecule fluorescence.[79] The nitro-aryl compound **75** was shown to be bioreduced in the presence of NTR to a highly fluorescent red-emitting fluorophore **76** by spectroscopic techniques. The NTR reaction was also characterised in bacterial cells with entire cells displaying 'turn on fluorescence'. Indeed, it was also possible to observe fluorescence on the single molecule level where incubation of **75** in *B. subtilis* at $<$nM levels resulted in fluorescent spots being observed to turn on and subsequently photobleach on the millisecond timescale giving detailed information on the localisation of the cytosolic and membrane bound NTR enzyme.

3. Azo linkages

Aside from the ubiquitous NTRs, both azoreductase (AZR) enzymes and the NADH:quinone oxidoreductases (also known as DT-diaphorases) are also known to be expressed at high levels under hypoxic conditions where they can effect the reduction of quinones and azo compounds.[80] The endogenous presence of AZR in hepatocellular carcinomas in humans has also resulted in their exploitation as hypoxia sensitive triggers in hypoxia activated enzyme therapies.[81] In order to investigate hypoxia-sensitive alternatives to nitroaromatic moieties Nagano and co-workers developed **77–79** (Fig. 35).[82] **77–79** consist of an

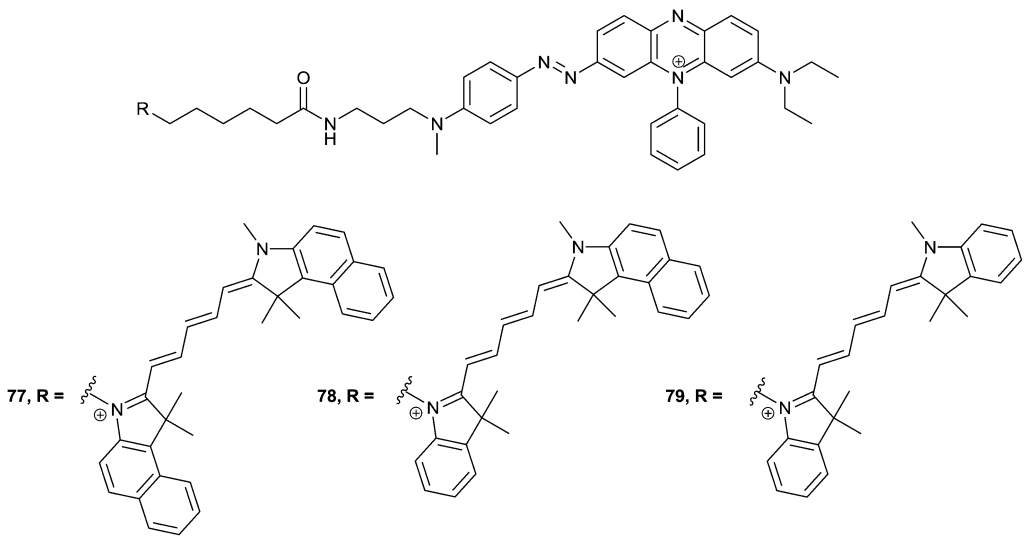

Fig. 35 Black Hole Quencher–dicarbocyanine conjugates **77–79**.

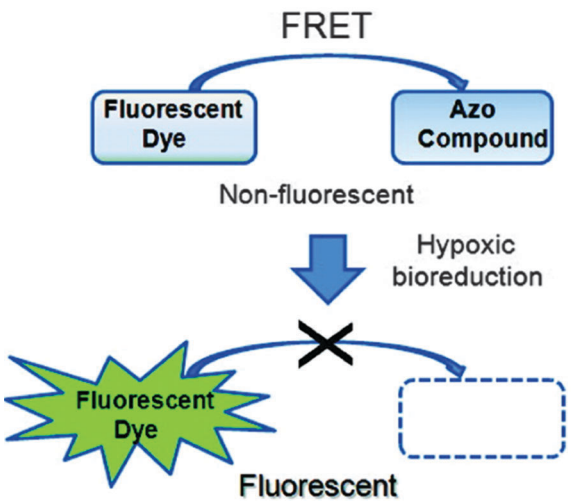

Fig. 36 The design strategy of the family of FRET based quencher fluorophores **77–79**. (Reproduced with permission from *J. Am. Chem. Soc.*, 2010, **132**, 15846–15848. © 2010 American Chemical Society).

azo based Black Hole Quencher© (BHQ) dye coupled with a near infrared (NIR) dicarbocyanine fluorophore. Due to the presence of Förster resonance energy transfer (FRET) between BHQ and the fluorophore, **77–79** exhibited extremely weak fluorescence (Fig. 36). However, a large fluorescence increase (50–100 fold) was triggered by the cleavage of the azo bond after enzymatic reactions using rat liver microsomes under hypoxic conditions. The ability of **77** to detect hypoxia was also demonstrated by the treatment of MCF-7 cells where the probe showed strong fluorescence only in cells incubated under hypoxic conditions. Moreover, **77** could also detect hypoxia *in vivo* using an ischemia model of the mouse liver where it was readily reduced in an ischemic liver while remaining non fluorescent in a normoxic liver.

A subsequent publication from Hanaoka, Nagano and co-workers reported a similar strategy in which two rhodamine based azo dyes, **80** and **81** were shown to be non-fluorescent in aqueous solution (Fig. 37).[83] The quenching involved was thought to be due to conformational rotation around the N=N bond resulting in an ultrafast radiationless decay profile of the excited state. Subsequent reductive cleavage of the azo bond, however, restored fluorescence by regenerating the original fluorophores 2Me rhodamine green (2Me RG) (λ_{max} = 520 nm) or 2Me Si-rhodamine 600 (2Me SiR 600) (λ_{max} = 613 nm) for **80** and **81** respectively.[84] The *in vitro* detection of hypoxia using rat liver microsomes, which contain various oxygen sensitive reductases, revealed a rapid increase in the fluorescence intensity of both **80** and **81** by 630-fold or 20-fold, respectively. Similarly, a time-dependent increase in emission, measured by both confocal fluorescence microscopy and flow-cytometric analysis, was observed in A549 cells treated with **80** and **81** under varying degrees of hypoxia where negligible emission was measured inside cells cultured under normoxic conditions. Perhaps most interestingly **80** was observed to function as a fluorescent probe capable of visualising retinal hypoxia in a rat model. Fluorescence imaging of a branch retinal artery occlusion (BRAO) treated with **80** resulted in emission intensity in the area of retinal hypoxia being considerably higher than that observed in a normoxic area (389.8% ± 189.8% *vs.* 100.0% ± 17.2% (mean ± SD)) (Fig. 37).

Qian *et al.* also took advantage of the azo linkage in the development of hypoxia probe **82** (Fig. 38).[85] **82** was designed to take advantage of the FRET pair of rhodamine B and azo-naphthalimide where reduction of the azo bond resulted in a

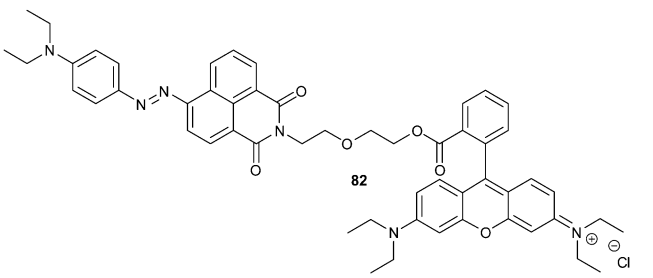

Fig. 38 Azo-naphthalimide–rhodamine B conjugate **82**.

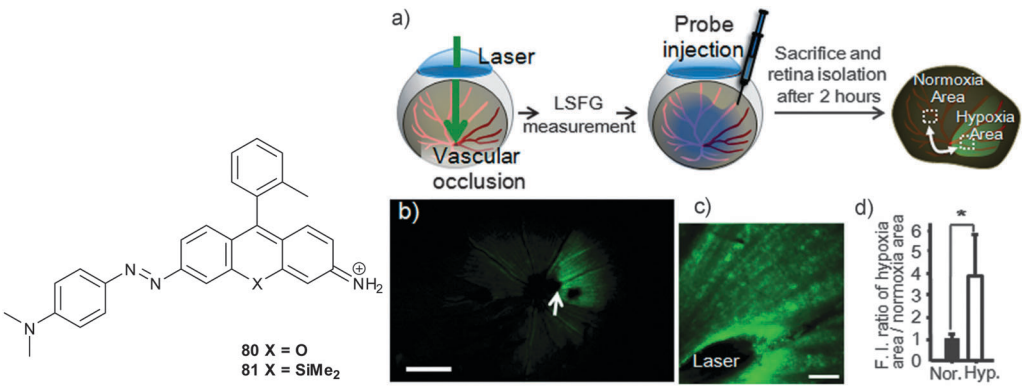

Fig. 37 Chemical structures of probes **80** and **81**. Fluorescence imaging of branch retinal artery occlusion (BRAO) in a rat model with **80**. (a) Hypoxia imaging method after BRAO. (b and c) Fluorescence imaging of the isolated retina two hours after treatment with a low (b)- or high (c)-magnification lens. Scale bars: 1 mm (b) and 100 mm (c). The arrow in (b) indicates the point of laser irradiation. (d) Comparison of the fluorescence intensities observed in hypoxic and normoxic areas. (Reproduced with permission from *Angew. Chem., Int. Ed.*, 2013, **52**, 13028–13032. © 2013 John Wiley and Sons).

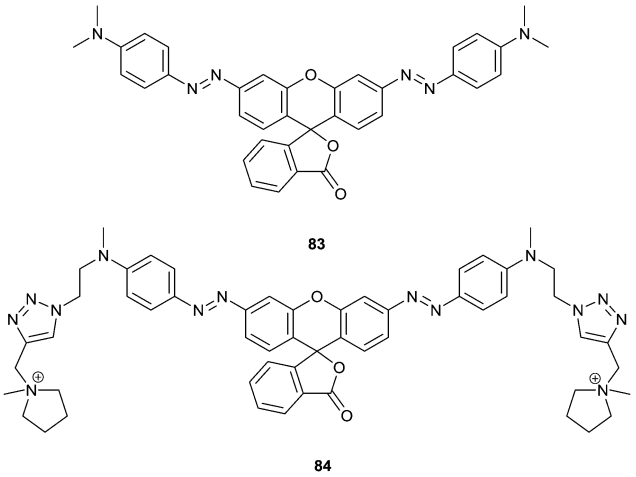

83

84

Fig. 39 Rhodamine based probe **83** and its water soluble analogue **84**.

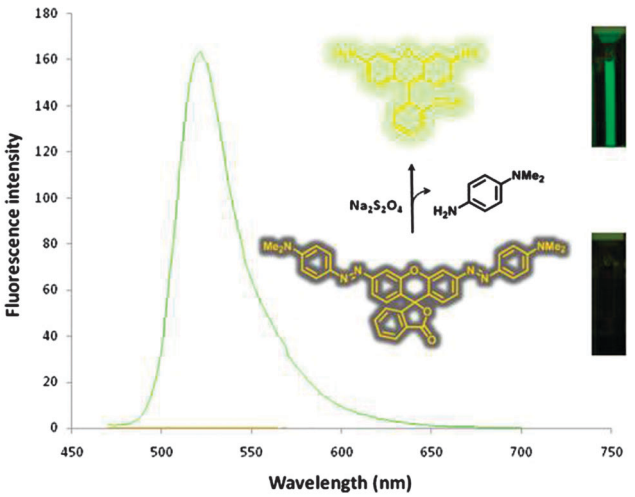

Fig. 40 Fluorescence emission spectra **83** in phosphate buffered saline + 1% DMSO before and after addition of sodium dithionite (100 equiv.). Inset: Images of the corresponding solutions under UV illumination conditions. (Reproduced from *Chem. Commun.*, 2013, **49**, 8815–8817. © 2013 Royal Society of Chemistry).

disruption of FRET and led to an enhancement of fluorescence at 581 nm. The reduction of **82** was effected by cytochrome P450 reductase and imaging in both normoxic and hypoxic HeLa cells demonstrated it's potential applicability as a sensitive biological imaging agent for hypoxia where there was a 9 fold variation in the ratio of fluorescence intensity between hypoxic and normoxic cells.

Romieu and co-workers developed the rhodamine based probe **83** and its water soluble analogue **84** for the selective detection of AZR in bacterial cultures (Fig. 39).[86] **83** was shown to exhibit a 'turn on' fluorescence response to mimicked AZR conditions using the biocompatible reducing agent sodium dithionate which resulted in a 250-fold increase in fluorescence at 520 nm (Fig. 40). A post-synthetic derivatisation approach allowed the assembly of **84** utilising copper-catalysed Huisgen 1,3-dipolar cycloaddition where the resultant positively charged tetralkylammonium groups, inferred both cell permeability and water solubility to the dye. *In vitro* activation of **84** was also demonstrated in a number of different bacterial strains (*E. coli*, *P. aeruginosa*, *S. aureus* and *E. faecalis*) where time-course experiments revealed a significant increase in *in cellulo* fluorescence of **84** in less than 3 hours. The fluorescent response of **83** was considerably lower, thought to be as a result its poor aqueous solubility.

Jayagopal and co-workers also utilised a FRET based strategy in the design of **85** a 'turn on' probe sensitive to AZR which is known to contribute to reductive stress in retinopathy (Fig. 41).[87] **85** displayed a 6.6 fold fluorescence increase when incubated in retinal neuronal cells (R28) and human retinal pigment epithelial cells (ARPE-19) for 4 h under hypoxic conditions. Additionally, **85** was demonstrated to successfully image focal hypoxia within laser-induced choroidal neovascularisation (LNCV) lesions (a mouse model for neovascular diseases such as macular degeneration) but not in adjacent healthy vascularised retinal tissue.

An original approach was taken by Bichenkova, Freeman and co-workers who published two reports on a pair of strained tetra-axial fluorescent probes for AZR activity **86** and **87** (Fig. 42).[88,89] The authors proposed that cleavage of the azo functionality prevented a dansyl (in the case of **86**) or a pyrene (in the case or **87**) moiety from forming a dimer complex. Using molecular dynamics simulations the authors suggested that upon reduction of the azo group a ring flip of the cyclohexane ring from a tetra-axial to a tetra-equatorial conformation occurred resulted in a change from dimer (555 nm) to blue-shifted monomer emission (448 nm) (Fig. 43(a)). Moreover, when *C. perfringens* were treated with **86** for 12 hours the resulting

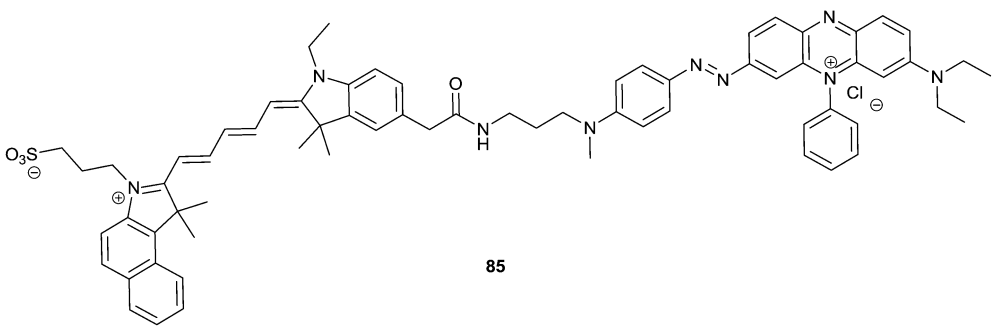

85

Fig. 41 FRET based probe **85**.

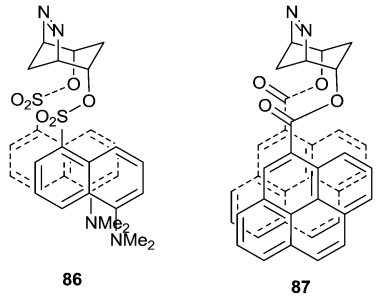

Fig. 42 Strained tetra-axial fluorescent probes for AZR activity **86** and **87**.

supernatant exhibited an 89% dimer emission decrease with a concomitant 89% increase in monomer fluorescence clearly demonstrating the applicability of **86** as an enzymatic biomarker for bacteria (Fig. 43(b)).

Sun, Li and co-workers recently took advantage of the azo linkage in the preparation of a family of iridium(III) complexes as phosphorescent probes for hypoxia.[90] The azo-based probes were found to be non-emissive in solution but upon treatment with rat liver microsomes under hypoxic conditions the phosphorescence intensity of each complex increased sharply with the fluorescence of **88** being particularly effective increasing by 58 fold. *In vitro* hypoxia experiments were conducted in 3D multicellular spheroids in order to mimic the hypoxic microenvironment of cancerous tumours.[91] Negligible phosphorescence was observed from each probe in small spheroids (150 μm in diameter) while large spheroids (500 μm in diameter) displayed bright phosphorescence in the hypoxic central region (Fig. 44).

4. Other functionalities

Quinones in general have the potential to undergo one-electron reduction by cytochrome P450 reductase which are available in high levels in hypoxic environments.[81] Tanabe and co-workers

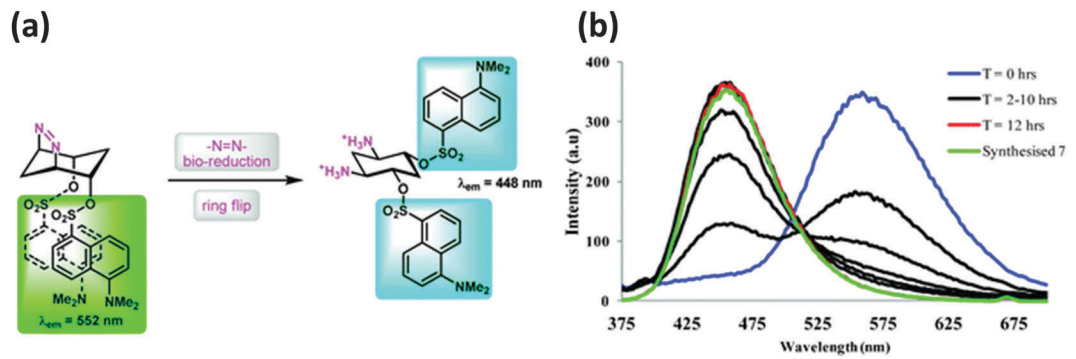

Fig. 43 (a) Reduction of the azo group in **86** results in a ring flip of the cyclohexane moiety to the more stable tetra-equatorial conformation. (b) Fluorescent changes associated with the bioreduction of **86** in the presence of *C. perfringens* cell culture supernatants known to contain azoreductive enzymes over 12 hours. (Reproduced from (a) *Chem. Commun.*, 2013, **49**, 8815–8817, (b) *Chem. Commun.*, 2012, **48**, 6393. © 2013 and 2012 Royal Society of Chemistry).

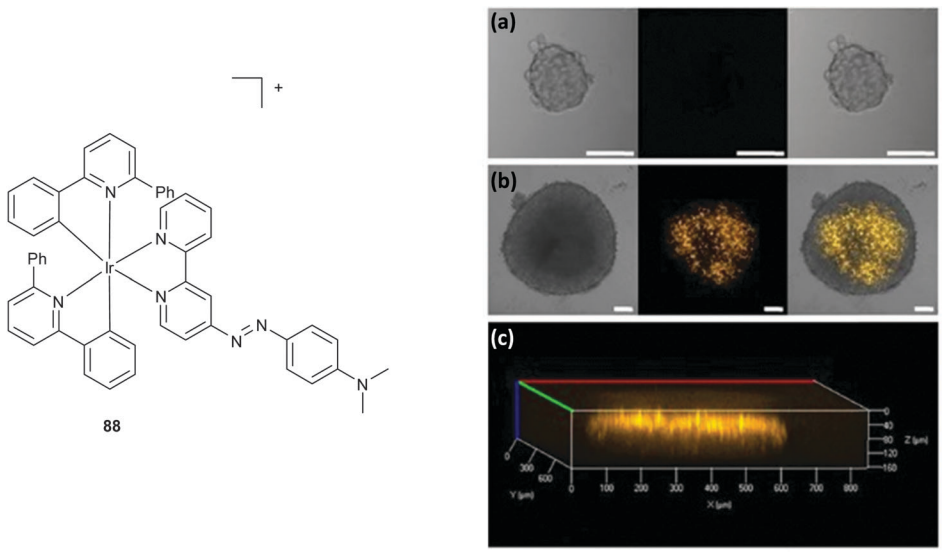

Fig. 44 Confocal images of 3D multicellular spheroids incubated with **88**. (a) Small 3D spheroids (b) large 3D spheroids (c) merged images of Z-stack images of an intact spheroid showing 3D biodistribution of **88** throughout. (Reproduced from *Sci. Rep.*, 2015, **5**, 14837. Shared under the Creative Commons Attribution 4.0 International License).

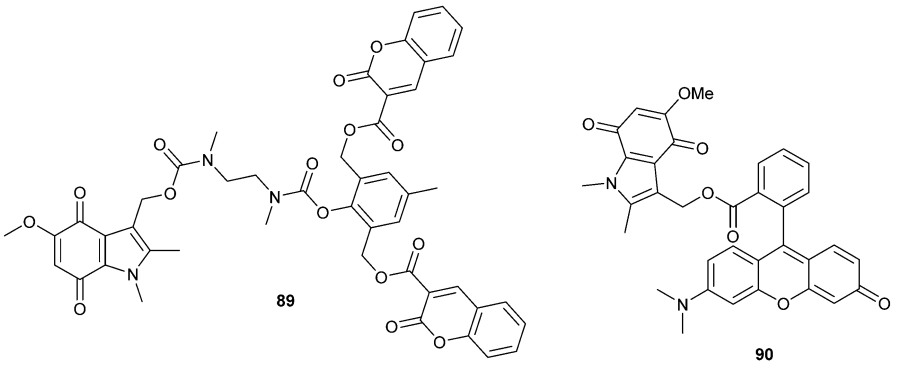

Fig. 45 Indolequinone conjugates **89** and **90**.

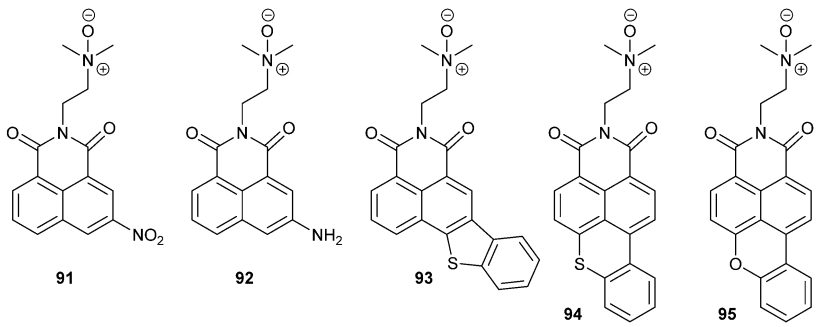

Fig. 46 Naphthalimide *N*-oxide derivatives **91–95**.

have reported a number of hypoxia sensitive molecules taking advantage of both reduction responsive fluorescent imaging agents and phosphorescent metal complexes.[92,93] Their first contribution in 2008 described a hypoxia-specific fluorescence probe **89** based on an indolequinone unit conjugated to two coumarin fluorophores (Fig. 45).[94] **89** showed weak fluorescence, attributed to the coumarin units being efficiently quenched by the indolequinone *via* a photoinduced electron transfer (PET) process. *Ab initio* calculations and laser flash photolysis both supported this theory where the results demonstrated that the photolysis of **89** induced electron transfer from the excited coumarin units to the indolequinone. One-electron reduction of **89** in the presence of NADPH and cytochrome P450 reductase under hypoxic conditions led to efficient decomposition and release of 2 molecules of coumarin-3-carboxylic acid. Similarly, lysate of the human fibrosarcoma cell line HT-1080 resulted in the same decomposition and in both cases led to intense fluorescence emission at 420 nm, four times as strong as that of the sample incubated under normoxic conditions. A subsequent report described the synthesis of **90** a rhodol–indolequinone conjugate that displayed weak fluorescence before bioreduction in the presence of cytochrome P450 reductase and NADPH released the rhodol fluorophore with intense fluorescence at 550 nm (Fig. 45).[95] Intracellular rhodol release was also revealed by *in vitro* fluorescence imaging of A549 cells under hypoxic conditions.

Both cytochrome P450 reductases and other haemoproteins have also been implicated in the reduction of the *N*-oxide functionality.[96] Although less explored in the context of fluorescence imaging a series of naphthalimide *N*-oxides (**91–95**) (Fig. 46) were reported by Qian and co-workers where their ability to bind to DNA as well as their potential as fluorescent

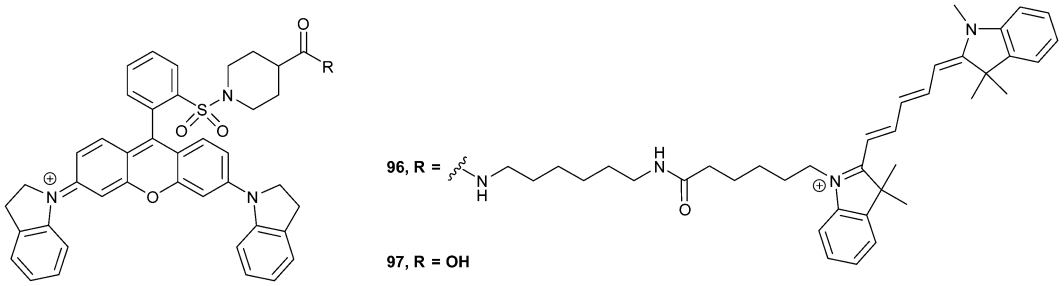

Fig. 47 Malachite green derivatives **96** and **97**.

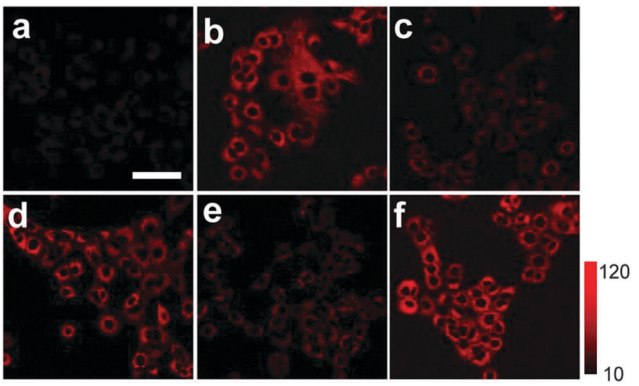

Fig. 48 Fluorescence confocal microscopic images of A549 cells treated with **96** and exposed to cycles of normoxia–hypoxia. Scale bar: 50 μm. (Reproduced with permission from *J. Am. Chem. Soc.*, 2012, **134**, 19588–19591. © 2012 American Chemical Society).

markers for hypoxia was evaluated.[97] Fluorescence image analysis indicated that **91** was particularly effective as a hypoxia marker where it displayed a hypoxic/normoxic fluorescence differential of 17 times when incubated for 4.5 h in V79 Chinese hamster cells. The authors suggested that this marked fluorescence increase was likely to be a result of a bis-bioreduction process where the *N*-oxide was reduced to the corresponding tertiary amine while the nitro group was also subsequently reduced to the corresponding primary amine.

Using an alternative approach Hanaoka, Nagano and co-workers have reported, to the best of my knowledge, the only example of a non-metal based reversible probe for hypoxia, **96** (Fig. 47).[98] The design of **96** was based on a FRET mechanism where a malachite green derivative **97** acted as a FRET acceptor and the NIR dicarbocyanine fluorophore **Cy5** as a FRET donor. **96** showed very weak emission under normoxic conditions, however, upon bioreduction and formation of a carbon centred radical, emission at 670 nm was 'switched on'. Electron spin resonance (ESR) spectroscopy confirmed the existence of a carbon centred radical under hypoxia with no signal being observed under normoxic conditions. The authors also demonstrated successful detection of repeated cycles of hypoxia–normoxia in live A549 human breast cancer cells where the fluorescence intensity rapidly decreased upon exposure of the cells to air (Fig. 48).

5. Conclusions

This Feature Article has demonstrated the diversity of fluorescent sensors and probes that have been developed for the detection not only of tumour hypoxia but also for reductase enzymes found in various genera of bacteria. The examples presented emphasise the versatility of this strategy where a wide range of structurally varied dyes have been utilised and have been applied both *in vitro* and *in vivo* for hypoxia detection and bacterial monitoring. Although significant progress has been made to date, further investigation is needed to exploit the full sensing potential of bioreductase enzymes and to understand the complex role played by them in hypoxic cells. In particular the development of reversible hypoxia probes, of which there are not many examples, will be an important consideration as the field moves in to the future. Within this context it is clear that fluorescent sensors like those described provide massive potential across a range of applications from medical diagnostics to environmental monitoring and beyond. Promisingly, with the many recent reports of hypoxia activated fluorescent agents it is obvious this is a rapidly expanding area gaining interest from research groups around the world. With significant research effort I envisage that the development of fluorescent probes for the detection of hypoxia will be recognised as an important field of research moving in to the future and continued investigation will lead to more diverse methods for hypoxia detection and tumour imaging.

Acknowledgements

The author wishes to acknowledge the help and support of Maynooth University and his Departmental colleagues.

References

1 J. M. Brown and W. R. Wilson, *Nat. Rev. Cancer*, 2004, **4**, 437–447.
2 W. R. Wilson and M. P. Hay, *Nat. Rev. Cancer*, 2011, **11**, 393–410.
3 W. A. Denny, *Eur. J. Med. Chem.*, 2001, **36**, 577–595.
4 A. J. Varghese, S. Gulyas and J. K. Mohindra, *Cancer Res.*, 1976, **36**, 3761–3765.
5 ClinicalTrials.gov Identifier: NCT, 01746979.
6 ClinicalTrials.gov Identifier: NCT, 01440088.
7 J. Kling, *Nat. Biotechnol.*, 2012, **30**, 381.
8 C. B. Brezden, L. Horn, R. A. McClelland and A. M. Rauth, *Biochem. Pharmacol.*, 1998, **56**, 335–344.
9 W. A. Denny, *Future Oncol.*, 2010, **6**, 419–428.
10 S. Kizaka-Kondoh and H. Konse-Nagasawa, *Cancer Sci.*, 2009, **100**, 1366–1373.
11 J. Pacheco-Torres, P. López-Larrubia, P. Ballesteros and S. Cerdán, *NMR Biomed.*, 2011, **24**, 1–16.
12 J. Wu, B. Kwon, W. Liu, E. V. Anslyn, P. Wang and J. S. Kim, *Chem. Rev.*, 2015, **115**, 7893–7943.
13 Z. Yang, J. Cao, Y. He, J. H. Yang, T. Kim, X. Peng and J. S. Kim, *Chem. Soc. Rev.*, 2014, **43**, 4563–4601.
14 X. Qian, Y. Xiao, Y. Xu, X. Guo, J. Qian and W. Zhu, *Chem. Commun.*, 2010, **46**, 6418–6436.
15 D. B. Papkovsky and R. I. Dmitriev, *Chem. Soc. Rev.*, 2013, **42**, 8700–8732.
16 A. K. Renfrew, *Metallomics*, 2014, **6**, 1324–1335.
17 G. N. Parkinson, J. V. Skelly and S. Neidle, *J. Med. Chem.*, 2000, **43**, 3624–3631.
18 E. M. Williams, R. F. Little, A. M. Mowday, M. H. Rich, J. V. E. Chan-Hyams, J. N. Copp, J. B. Smaill, A. V. Patterson and D. F. Ackerley, *Biochem. J.*, 2015, **471**, 131–153.
19 P. L. Olive and R. E. Durand, *Cancer Res.*, 1983, **43**, 3276–3280.
20 P. L. Olive, *Int. J. Radiat. Oncol., Biol., Phys.*, 1984, **10**, 1357–1360.
21 P. L. Olive, *Int. J. Radiat. Oncol., Biol., Phys.*, 1985, **11**, 1947–1954.
22 P. L. Olive, J. S. Rasey and R. E. Durand, *Radiat. Res.*, 1986, **105**, 105–114.
23 R. J. Hodgkiss, A. C. Begg, R. W. Middleton, J. Parrick, M. R. L. Stratford, P. Wardman and G. D. Wilson, *Biochem. Pharmacol.*, 1991, **41**, 533–541.
24 A. C. Begg, E. L. Engelhardt, R. J. Hodgkiss, N. J. McNally, N. H. A. Terry and P. Wardman, *Br. J. Radiol.*, 1983, **56**, 970–973.
25 P. Wardman, E. D. Clarke, R. J. Hodgkiss, R. W. Middleton, J. Parrick and M. R. L. Stratford, *Int. J. Radiat. Oncol., Biol., Phys.*, 1984, **10**, 1347–1351.

26 M. R. L. Stratford, E. D. Clarke, R. J. Hodgkiss, R. W. Middleton and P. Wardman, *Int. J. Radiat. Oncol., Biol., Phys.*, 1984, **10**, 1353–1356.
27 A. C. Begg, R. J. Hodgkiss, N. J. McNally, R. W. Middleton, M. R. Stratford and N. H. Terry, *Br. J. Radiol.*, 1985, **58**, 645–654.
28 R. J. Hodgkiss, G. W. Jones, A. Long, R. W. Middleton, J. Parrick, M. R. L. Stratford, P. Wardman and G. D. Wilson, *J. Med. Chem.*, 1991, **34**, 2268–2274.
29 R. J. Hodgkiss, R. W. Middleton, J. Parrick, H. K. Rami, P. Wardman and G. D. Wilson, *J. Med. Chem.*, 1992, **35**, 1920–1926.
30 R. J. Hodgkiss, J. Parrick, M. Porssa and M. R. L. Stratford, *J. Med. Chem.*, 1994, **37**, 4352–4356.
31 Y. Liu, Y. Xu, X. Qian, J. Liu, L. Shen, J. Li and Y. Zhang, *Bioorg. Med. Chem.*, 2006, **14**, 2935–2941.
32 Y. Liu, Y. Xu, X. Qian, Y. Xiao, J. Liu, L. Shen, J. Li and Y. Zhang, *Bioorg. Med. Chem. Lett.*, 2006, **16**, 1562–1566.
33 M. Dai, W. Zhu, Y. Xu, X. Qian, Y. Liu, Y. Xiao and Y. You, *J. Fluoresc.*, 2008, **18**, 591–597.
34 W. Zhu, M. Dai, Y. Xu and X. Qian, *Bioorg. Med. Chem.*, 2008, **16**, 3255–3260.
35 L. Cui, Y. Zhong, W. Zhu, Y. Xu, Q. Du, X. Wang, X. Qian and Y. Xiao, *Org. Lett.*, 2011, **13**, 928–931.
36 T. Guo, L. Cui, J. Shen, W. Zhu, Y. Xu and X. Qian, *Chem. Commun.*, 2013, **49**, 10820–10822.
37 E. Nakata, Y. Yukimachi, H. Kariyazono, S. Im, C. Abe, Y. Uto, H. Maezawa, T. Hashimoto, Y. Okamoto and H. Hori, *Bioorg. Med. Chem.*, 2009, **17**, 6952–6958.
38 S. M. Evans, K. Kim, C. E. Moore, M. I. Uddin, M. E. Capozzi, J. R. Craft, G. A. Sulikowski and A. Jayagopal, *Bioconjugate Chem.*, 2014, **25**, 2030–2037.
39 S. Bhaumik, T. V. Sekar, J. Depuy, J. Klimash and R. Paulmurugan, *Gene Ther.*, 2012, **19**, 295–302.
40 E. McCormack, E. Silden, R. M. West, T. Pavlin, D. R. Micklem, J. B. Lorens, B. E. Haug, M. E. Cooper and B. T. Gjertsen, *Cancer Res.*, 2013, **73**, 1276–1286.
41 B. G. M. Youssif, K. Okuda, T. Kadonosono, O. I. A. R. Salem, A. A. M. Hayallah, M. A. Hussein, S. Kizaka-Kondoh and H. Nagasawa, *Chem. Pharm. Bull.*, 2012, **60**, 402–407.
42 K. Okuda, Y. Okabe, T. Kadonosono, T. Ueno, B. G. M. Youssif, S. Kizaka-Kondoh and H. Nagasawa, *Bioconjugate Chem.*, 2012, **23**, 324–329.
43 C. Pavlik, N. C. Biswal, F. C. Gaenzler, M. D. Morton, L. T. Kuhn, K. P. Claffey, Q. Zhu and M. B. Smith, *Dyes Pigm.*, 2011, **89**, 9–15.
44 N. C. Biswal, C. Pavlik, M. B. Smith, A. Aguirre, Y. Xu, S. Zanganeh, L. T. Kuhn, K. P. Claffey and Q. Zhu, *J. Biomed. Opt.*, 2011, **16**, 066009.
45 Y. Xu, S. Zanganeh, I. Mohammad, A. Aguirre, T. Wang, Y. Yang, L. Kuhn, M. B. Smith and Q. Zhu, *J. Biomed. Opt.*, 2013, **18**, 066009.
46 F. Zhou, S. Zanganeh, I. Mohammad, C. Dietz, A. Abuteen, M. B. Smith and Q. Zhu, *Org. Biomol. Chem.*, 2015, **13**, 11220–11227.
47 A. Abuteen, F. Zhou, C. Dietz, I. Mohammad, M. B. Smith and Q. Zhu, *Dyes Pigm.*, 2016, **126**, 251–260.
48 I. J. Stratford, C. Williamson and C. Hardy, *Br. J. Cancer*, 1981, **44**, 109–116.
49 K. Xu, F. Wang, X. Pan, R. Liu, J. Ma, F. Kong and B. Tang, *Chem. Commun.*, 2013, **49**, 2554–2556.
50 Y. Shi, S. Zhang and X. Zhang, *Analyst*, 2013, **138**, 1952–1955.
51 Y. Li, Y. Sun, J. Li, Q. Su, W. Yuan, Y. Dai, C. Han, Q. Wang, W. Feng and F. Li, *J. Am. Chem. Soc.*, 2015, **137**, 6407–6416.
52 C. Xue, Y. Lei, S. Zhang and Y. Sha, *Anal. Methods*, 2015, **7**, 10125–10128.
53 D. Zhu, L. Xue, G. Li and H. Jiang, *Sens. Actuators, B*, 2016, **222**, 419–424.
54 J. Yuan, Y.-Q. Xu, N.-N. Zhou, R. Wang, X.-H. Qian and Y.-F. Xu, *RSC Adv.*, 2014, **4**, 56207–56210.
55 Z. Li, X. Li, X. Gao, Y. Zhang, W. Shi and H. Ma, *Anal. Chem.*, 2013, **85**, 3926–3932.
56 Z. Li, X. Gao, W. Shi, X. Li and H. Ma, *Chem. Commun.*, 2013, **49**, 5859–5861.
57 Q.-Q. Wan, X.-H. Gao, X.-Y. He, S.-M. Chen, Y.-C. Song, Q.-Y. Gong, X.-H. Li and H.-M. Ma, *Chem. – Asian J.*, 2014, **9**, 2058–2062.
58 Z. Li, X. He, Z. Wang, R. Yang, W. Shi and H. Ma, *Biosens. Bioelectron.*, 2015, **63**, 112–116.
59 J. Xu, S. Sun, Q. Li, Y. Yue, Y. Li and S. Shao, *Analyst*, 2015, **140**, 574–581.
60 S. Wang, H. Liu, J. Mack, J. Tian, B. Zou, H. Lu, Z. Li, J. Jiang and Z. Shen, *Chem. Commun.*, 2015, **51**, 13389–13392.
61 S. Debieu and A. Romieu, *Org. Biomol. Chem.*, 2015, **13**, 10348–10361.
62 N. Saini, R. Varshney, A. K. Tiwari, A. Kaul, M. P. S. Ishar and A. K. Mishra, *RSC Adv.*, 2015, **5**, 97102–97112.
63 Q. Jiang, Z. Zhang, J. Lu, Y. Huang, Z. Lu, Y. Tan and Q. Jiang, *Bioorg. Med. Chem.*, 2013, **21**, 7735–7741.
64 A. Rajapakse and K. S. Gates, *J. Org. Chem.*, 2012, **77**, 3531–3537.
65 A. Rajapakse, C. Linder, R. D. Morrison, U. Sarkar, N. D. Leigh, C. L. Barnes, J. S. Daniels and K. S. Gates, *Chem. Res. Toxicol.*, 2013, **26**, 555–563.
66 A. V. Patterson, D. M. Ferry, S. J. Edmunds, Y. Gu, R. S. Singleton, K. Patel, S. M. Pullen, K. O. Hicks, S. P. Syddall, G. J. Atwell, S. Yang, W. A. Denny and W. R. Wilson, *Clin. Cancer Res.*, 2007, **13**, 3922–3932.
67 J. Su, C. P. Guise and W. R. Wilson, *Biochem. J.*, 2013, **452**, 79–86.
68 O. Mazuryk, M. Maciuszek, G. Stochel, F. Suzenet and M. Brindell, *J. Inorg. Biochem.*, 2014, **134**, 83–91.
69 O. Mazuryk, F. Suzenet, C. Kieda and M. Brindell, *Metallomics*, 2015, **7**, 553–566.
70 J. Zhang, H.-W. Liu, X.-X. Hu, J. Li, L.-H. Liang, X.-B. Zhang and W. Tan, *Anal. Chem.*, 2015, **87**, 11832–11839.
71 P. Lehouritis, C. Springer and M. Tangney, *J. Controlled Release*, 2013, **170**, 120–131.
72 S. Michael, C. Michelle, L. Panos and T. Mark, *Curr. Gene Ther.*, 2015, **15**, 277–288.
73 A. G. Vorobyeva, M. Stanton, A. Godinat, K. B. Lund, G. G. Karateev, K. P. Francis, E. Allen, J. G. Gelovani, E. McCormack, M. Tangney and E. A. Dubikovskaya, *PLoS One*, 2015, **10**, e0131037.
74 W. B. Porterfield, K. A. Jones, D. C. McCutcheon and J. A. Prescher, *J. Am. Chem. Soc.*, 2015, **137**, 8656–8659.
75 R. H. F. Wong, T. Kwong, K.-H. Yau and H. Y. Au-Yeung, *Chem. Commun.*, 2015, **51**, 4440–4442.
76 M. Cellier, O. J. Fabrega, E. Fazackerley, A. L. James, S. Orenga, J. D. Perry, V. L. Salwatura and S. P. Stanforth, *Bioorg. Med. Chem.*, 2011, **19**, 2903–2910.
77 M. Cellier, A. Gignoux, A. L. James, S. Orenga, J. D. Perry, S. N. Robinson, S. P. Stanforth and G. Turnbull, *Bioorg. Med. Chem. Lett.*, 2015, **25**, 5694–5698.
78 J. Bae, L. E. McNamara, M. A. Nael, F. Mahdi, R. J. Doerksen, G. L. Bidwell, N. I. Hammer and S. Jo, *Chem. Commun.*, 2015, **51**, 12787–12790.
79 M. K. Lee, J. Williams, R. J. Twieg, J. Rao and W. E. Moerner, *Chem. Sci.*, 2013, **4**, 220–225.
80 S. Zbaida, *Enzyme Systems that Metabolise Drugs and Other Xenobiotics*, 2001, p. 555.
81 A. K. Sinhababu and D. R. Thakker, *Adv. Drug Delivery Rev.*, 1996, **19**, 241–273.
82 K. Kiyose, K. Hanaoka, D. Oushiki, T. Nakamura, M. Kajimura, M. Suematsu, H. Nishimatsu, T. Yamane, T. Terai, Y. Hirata and T. Nagano, *J. Am. Chem. Soc.*, 2010, **132**, 15846–15848.
83 W. Piao, S. Tsuda, Y. Tanaka, S. Maeda, F. Liu, S. Takahashi, Y. Kushida, T. Komatsu, T. Ueno, T. Terai, T. Nakazawa, M. Uchiyama, K. Morokuma, T. Nagano and K. Hanaoka, *Angew. Chem., Int. Ed.*, 2013, **52**, 13028–13032.
84 Y. Kushida, K. Hanaoka, T. Komatsu, T. Terai, T. Ueno, K. Yoshida, M. Uchiyama and T. Nagano, *Bioorg. Med. Chem. Lett.*, 2012, **22**, 3908–3911.
85 Q. Cai, T. Yu, W. Zhu, Y. Xu and X. Qian, *Chem. Commun.*, 2015, **51**, 14739–14741.
86 A. Chevalier, C. Mercier, L. Saurel, S. Orenga, P.-Y. Renard and A. Romieu, *Chem. Commun.*, 2013, **49**, 8815–8817.
87 M. I. Uddin, S. M. Evans, J. R. Craft, L. J. Marnett, M. J. Uddin and A. Jayagopal, *ACS Med. Chem. Lett.*, 2015, **6**, 445–449.
88 N. J. W. Rattray, W. A. Zalloum, D. Mansell, J. Latimer, C. H. Schwalbe, A. J. Blake, E. V. Bichenkova and S. Freeman, *Chem. Commun.*, 2012, **48**, 6393–6395.
89 N. J. W. Rattray, W. A. Zalloum, D. Mansell, J. Latimer, M. Jaffar, E. V. Bichenkova and S. Freeman, *Tetrahedron*, 2013, **69**, 2758–2766.
90 L. Sun, G. Li, X. Chen, Y. Chen, C. Jin, L. Ji and H. Chao, *Sci. Rep.*, 2015, **5**, 14837.

91 F. Hirschhaeuser, H. Menne, C. Dittfeld, J. West, W. Mueller-Klieser and L. A. Kunz-Schughart, *J. Biotechnol.*, 2010, **148**, 3–15.
92 A. Son, A. Kawasaki, D. Hara, T. Ito and K. Tanabe, *Chem. – Eur. J.*, 2015, **21**, 2527–2536.
93 D. Hara, H. Komatsu, A. Son, S.-i. Nishimoto and K. Tanabe, *Bioconjugate Chem.*, 2015, **26**, 645–649.
94 K. Tanabe, N. Hirata, H. Harada, M. Hiraoka and S.-i. Nishimoto, *ChemBioChem*, 2008, **9**, 426–432.
95 H. Komatsu, H. Harada, K. Tanabe, M. Hiraoka and S.-i. Nishimoto, *Med. Chem. Commun.*, 2010, **1**, 50–53.
96 C. Hugo and G. Mercedes, *Mini-Rev. Med. Chem.*, 2001, **1**, 219–231.
97 H. Yin, W. Zhu, Y. Xu, M. Dai, X. Qian, Y. Li and J. Liu, *Eur. J. Med. Chem.*, 2011, **46**, 3030–3037.
98 S. Takahashi, W. Piao, Y. Matsumura, T. Komatsu, T. Ueno, T. Terai, T. Kamachi, M. Kohno, T. Nagano and K. Hanaoka, *J. Am. Chem. Soc.*, 2012, **134**, 19588–19591.

